RESEARCH ARTICLE

An Isoform-Specific RUNX1C–BTG2 Axis Governs AML Quiescence and Chemoresistance

Cuijuan Han[1], Zhiping Zhang[2], Edie I. Crosse[3], Sogand Sajedi[4], Bin Lu[5], Xiyue Wang[1,6], Sadik Karma[1,6], Mitch Kostich[1], Sakthi Harini Rajendran[1,6], Dylan B. Udy[3], Steven Chen[2], Alexander Arnuk[1], Abimbola Eunice Lawal[1], Kayla R. Koenig[1], Meryl McKenna[1], Patrick K. Reville[4], Hussein A. Abbas[4], Omar Abdel-Wahab[7], Pedro Miura[2,8], Robert K. Bradley[3,9], and Eric Wang[1,2,8]

ABSTRACT Aberrant levels or structures of RNA isoforms are a hallmark of many cancers, including acute myeloid leukemia (AML), yet their role in AML chemoresistance remains unclear. We conducted a paired analysis of RNA isoform changes in patients with AML before therapy and at relapse after chemotherapy and identified intragenic DNA methylation at the proximal promoter of the transcription factor *RUNX1*, which resulted in elevated expression of the long-isoform *RUNX1C* through its alternative distal promoter. The unique N-terminal region of RUNX1C orchestrated an isoform-specific transcriptional program that promoted chemoresistance, with its direct target *BTG2* playing a role in chemotherapy resistance. BTG2 promoted rRNA deadenylation, resulting in decreased mRNA expression and stability. Deletion of rRNAs increased cellular quiescence. Moreover, RNA-based targeting of *RUNX1C* reactivated quiescent leukemia cells and enhanced chemotherapy efficacy. These findings delineated an isoform-specific transcriptional circuit that governed chemotherapy response, providing a potential therapeutic strategy to mitigate AML recurrence.

SIGNIFICANCE: This study identifies RUNX1C as a contributor to AML chemoresistance and an inducer of quiescence through BTG2. Targeting RUNX1C with RNA-based approaches disrupts this state and improves chemotherapy response, highlighting RUNX1C inhibition as a promising strategy to overcome resistance and enhance treatment efficacy in AML.

INTRODUCTION

Acute myeloid leukemia (AML) is the most prevalent form of acute leukemia in adults. Despite the high initial remission rates with the standard "7 + 3" chemotherapy regimen (cytarabine with an anthracycline), approximately 50% to 80% of patients with AML will experience relapse within 5 years with poor clinical outcomes, and older individuals experience higher recurrence rates (1). Relapse after remission can occur due to a rare population of quiescent leukemic cells that persist during chemotherapy, which can ultimately serve as a reservoir for minimal residual disease (2). The failure of current treatments to effectively eradicate minimal residual disease underscores the critical need to understand the molecular basis of AML quiescence, which may inform the development of future therapeutic modalities.

Large-scale genomic sequencing studies have shown a scarcity of mutations in patients with relapsed AML (3), implying the contribution of nongenetic alterations that mediate therapeutic resistance, thus making the clinical management of AML challenging (4–6). Altered RNA splicing has been previously implicated in AML progression and therapeutic resistance (7, 8) irrespective of mutations (9, 10). Here, we directly characterized the alternative splicing landscape in patients with relapsed AML, which remains poorly understood. Transcription factors (TF) represent one of the most ubiquitous gene families that undergo pre-mRNA splicing to generate protein isoforms or "proteoforms" that differ in their DNA-binding domains or other protein regions (11). The Runt-related TF RUNX1 (also known as *AML1*) is a master regulator of hematopoiesis and is essential for primitive blood development (12). In adult hematopoiesis, RUNX1 is dispensable (13), as evidenced by the frequent onset of myeloid malignancies caused by loss-of-function *RUNX1* mutations or fusion with other proteins through chromosomal translocations (e.g., *AML1–ETO*; ref. 14). *RUNX1* encodes three annotated spliced isoforms (A, B, and C) that are differentially expressed during normal development (15) and disease states (16), implicating isoform-dependent functions. However, to the best of our knowledge, the mechanistic importance of RUNX1 isoforms in AML drug resistance has not yet been previously characterized.

Here, we provide a comprehensive and longitudinal analysis of the RNA isoform landscape in patients with AML before treatment and at relapse after chemotherapy. We found that the long isoform of *RUNX1*, *RUNX1C*, was upregulated in patients with relapsed AML and contributed to chemoresistance. Mechanistically, RUNX1C promoted AML quiescence by regulating a distinct transcriptional program that includes direct targets, including BTG antiproliferation factor 2 (*BTG2*), which we have shown can modulate the deadenylation

[1]The Jackson Laboratory for Genomic Medicine, Farmington, Connecticut. [2]Department of Genetics and Genome Sciences, UConn Health, Farmington, Connecticut. [3]Public Health Sciences and Basic Sciences Divisions, Fred Hutchinson Cancer Research Center, Seattle, Washington. [4]Department of Leukemia, The University of Texas MD Anderson Cancer Center, Houston, Texas. [5]Sanford Burnham Prebys Medical Discovery Institute, San Diego, California. [6]Graduate Program in Genetics and Development, UConn Health, Farmington, Connecticut. [7]Molecular Pharmacology Program, Sloan Kettering Institute, Memorial Sloan Kettering Cancer Center, New York, New York. [8]Institute for Systems Genomics, University of Connecticut Health Center, Farmington, Connecticut. [9]Department of Genome Sciences, University of Washington, Seattle, Washington.

Corresponding Author: Eric Wang, The Jackson Laboratory for Genomic Medicine, 10 Discovery Drive, Farmington, CT 06032. E-mail: eric.wang@jax.org

Blood Cancer Discov 2025;6:464–83

doi: 10.1158/2643-3230.BCD-24-0327

of rRNAs, leading to reduced protein synthesis. RNA-based targeting of *RUNX1C* isoform reactivated quiescent leukemia cells and enhanced chemotherapy efficacy. Collectively, these findings revealed an isoform-specific transcriptional program of RUNX1C that mediated leukemia quiescence via BTG2. Moreover, we showed that BTG2 regulated the deadenylation of rRNAs and that targeting *RUNX1C* allowed AML cells to reenter cell cycle and improved chemotherapy responsiveness.

RESULTS

Transcriptome-Wide Isoform Profiling in Relapsed AML Samples

To characterize changes in isoform abundance and alternative splicing (AS) underlying AML relapse after chemotherapy, we performed both supervised analyses of transcript abundance (17) and AS (18) using published RNA sequencing (RNA-seq) data from 19 matched AML bone marrow specimens collected at diagnosis and relapse after combination chemotherapy (Fig. 1A and B; Supplementary Fig. S1A; Supplementary Table S1; ref. 4). In the relapsed cohort, we identified 5,859 transcripts that were significantly upregulated ($\log_2$ fold change >0.75) in relapsed samples compared with 1,748 transcripts that were downregulated ($P < 0.05$, $\log_2$ fold change <−0.75; Fig. 1B). In our splicing analysis, we discerned approximately 670 significant differential spliced events that spanned six main types of AS events: cassette exon, alternative 5′ splice sites (ss), alternative 3′ ss, mutually exclusive exons, retained introns, and tandem 3′ untranslated regions using the FDR of <0.05 and Δpercent spliced in >10% (Supplementary Fig. S1B). The most common type of splicing change in patients with relapsed AML was cassette exon splicing (48.9%), followed by tandem 3′ untranslated regions (15.5%) and alternative 5′ ss usage (12.6%; Supplementary Fig. S1C and S1D). Notably, we observed a global increase in cassette exon inclusion events ($n = 163$) compared with repressed exons ($n = 44$) in AML relapse (Supplementary Fig. S1C). These cassette exons that were more inclusive in relapsed patients were enriched for GC-rich motifs (Supplementary Fig. S1E). Overlapping both analyses identified that the long isoform of RUNX1 (also referred to as *RUNX1C*) was significantly upregulated in relapsed AML samples but not in its other annotated isoforms, *RUNX1A* and *RUNX1B* (Fig. 1C). Consistent with these findings, we observed the inclusion of RUNX1 exons 1 and 2, which are unique to the *RUNX1C* transcript (Δpercent spliced in = 0.17), as one of the top cassette exon changes identified in our splicing analysis. This was observed in 11 of 19 relapsed patients (Fig. 1D; Supplementary Fig. S1F).

Aberrant DNA Methylation of Alternative Promoters Regulates RUNX1C Expression

Alternative promoters modulate the transcription of distinct RNA isoforms, which are often dysregulated in tumors (19), but the regulation of which are not fully explored in AML. The distal P1 promoter of RUNX1 drives the expression of the longest isoform, *RUNX1C*, which encodes a poorly characterized N-terminal region, whereas the proximal P2 promoter drives the expression of *RUNX1A* and *RUNX1B* (20). Previous reports indicate that alternative promoter methylation and TF binding to RUNX1 P1 and P2 promoters occur during embryonic development, resulting in differential expression of RUNX1 isoforms (20–22), suggesting that distinct TF regulatory mechanisms may govern activity at these promoters in relapse. To explore potential transcriptional regulators of RUNX1 isoform expression, we first performed TF motif analysis of the P1 and P2 promoters of *RUNX1*, which identified differentially enriched TFs binding to each promoter (Supplementary Fig. S2A). Next, to determine whether alternative promoter methylation of RUNX1 is dysregulated during AML relapse, we analyzed enhanced reduced representation bisulfite sequencing data from the same cohort study of patients with AML (4). Using the methylKit, we identified significant (FDR <0.05) differentially methylated regions for each patient with relapse–diagnosis paired AML across all CpG probes within the P2 promoter at relapse and diagnosis [Δ%5-methylcytosine (5-mc)]. Compared with pretreatment, a subset of patients with relapsed AML showed significantly elevated intragenic DNA methylation at the P2 proximal promoter, which has been shown to drive the *RUNX1A* and *RUNX1B* isoform expression (Fig. 1E; Supplementary Fig. S2B; Supplementary Table S1; refs. 23–25). As increased promoter methylation generally represses transcription, we hypothesized that hypermethylation of the P2 promoter may further increase transcription at the P1 distal promoter, which has been shown to regulate long-isoform *RUNX1C*. To test this hypothesis, we used a catalytically inactive Cas9 protein fused to Dnmt3a to allow site-specific DNA methylation and repression of the P2 proximal promoter in MOLM-13 cells (Fig. 1F; Supplementary Fig. S2C). Bisulfite Sanger sequencing confirmed that single-guide RNA (sgRNA) targeting the P2 promoter showed increased methylation (6.75%) compared with the control sgRNA (2.5%; Fig. 1G). We observed that dCas9-Dnmt3a–mediated *de novo* methylation of the P2 promoter of RUNX1 resulted in decreased *RUNX1A/B* levels but upregulated *RUNX1C* mRNA expression compared with the catalytic inactive form of Dnmt3a and dCas9 only (Fig. 1H; Supplementary Fig. S2D). Conversely, dCas9 Tet1 resulted in increased RUNX1A/B expression and *RUNX1C* levels (Supplementary Fig. S2E). Together, these data suggest a relationship between aberrant DNA methylation of alternative promoters and the regulation of TF isoforms associated with AML relapse.

Long-Isoform RUNX1C Modulates Chemotherapy Response in AML

To study the relationship between RUNX1C expression and chemotherapy response, we assessed two patient-derived xenografts (PDX) of AML and six genetically diverse human AML cell lines (U937, MOLM-13, MOLM-14, NOMO-1, KG-1a, and THP-1). We observed that the AML cell lines KG-1a, THP-1, and NOMO-1 displayed elevated RUNX1B and RUNX1C protein levels, which correlated with higher IC_{50} values (50% of maximal inhibitory effect concentration) when treated with the commonly used chemotherapeutic agents, cytarabine or idarubicin (Fig. 2A–C). By contrast, the AML cell lines U937, MOLM-13, and MOLM-14 showed lower RUNX1B/C protein levels and higher chemosensitivity (Fig. 2A–C). Next, we performed direct long-read sequencing (LR-seq) using Oxford

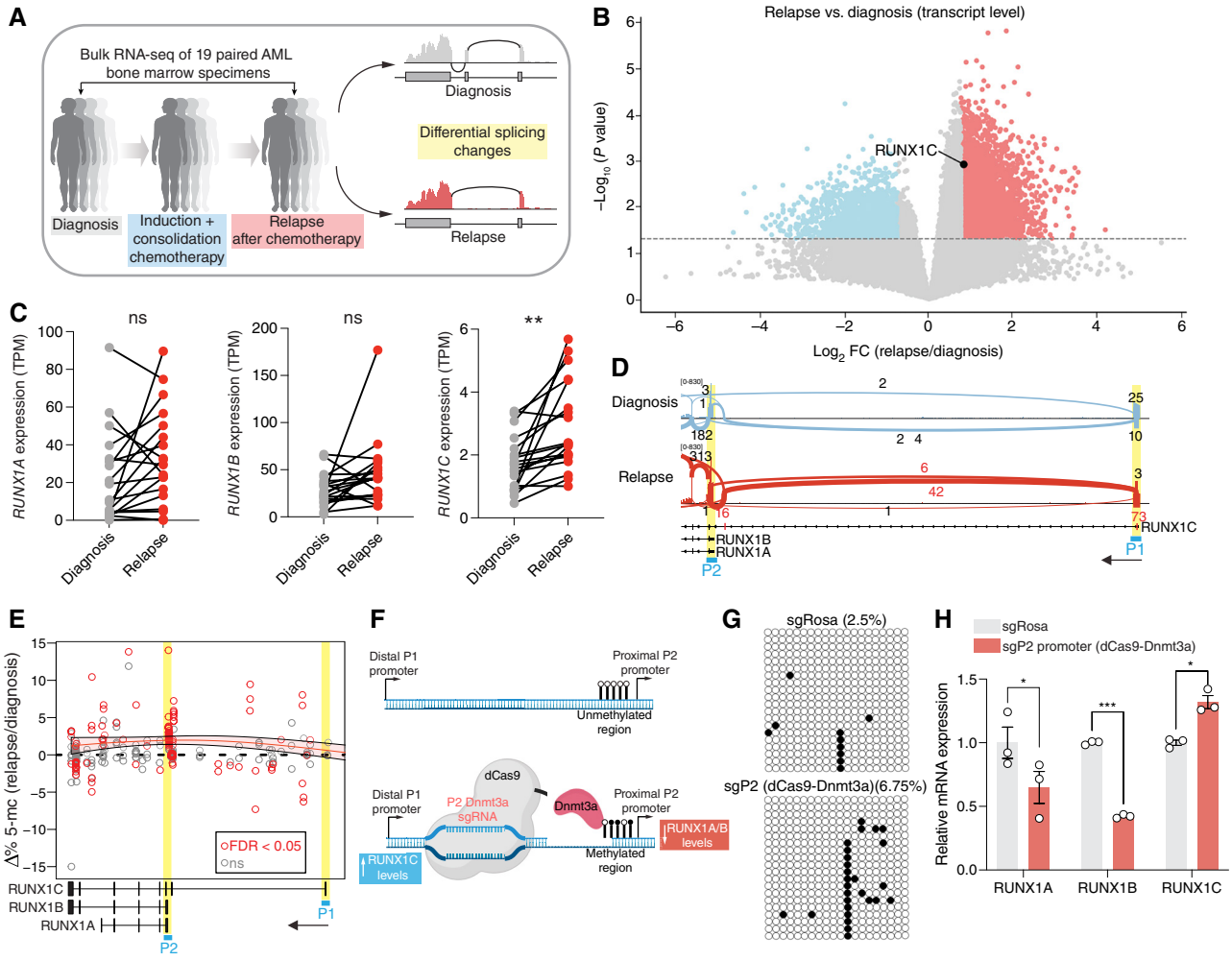

Figure 1. Alternative promoter methylation regulates isoform-dependent expression in AML relapse. **A,** Isoform and AS analyses of RNA-seq data from bone marrow samples of 19 paired patients with AML at diagnosis (pretreatment) and following relapse after combination chemotherapy treatment. **B,** Volcano plot analysis of all transcripts in relapsed vs. diagnosis in patients with AML. Significant upregulated transcripts are denoted in red (log_2 fold change >0.75, $P < 0.05$) and downregulated transcripts are denoted in cyan (log_2 fold change <−0.75, $P < 0.05$). **C,** RUNX1 isoform transcript analysis from (**B**) in relapsed vs. diagnosis. **D,** Sashimi plot illustrating cassette exon inclusion of *RUNX1* exons 1 and 2 in relapsed patients vs. diagnosis patients. Arrow represents the direction of the gene. **E,** Each dot represents an individual CpG probe, depicting the mean Δ5-mc (relapse vs. diagnosis) across 19 patients at its corresponding CpG site. For each patient with AML, Δ5-mc was calculated as the difference in methylation proportion between relapse and diagnosis. Significant regions (FDR <0.05) are highlighted in red circles. The distal promoter P1 and proximal promoter P2 are as indicated. *P* values were calculated using χ^2 statistics and FDRs calculated using the Benjamini–Yekutieli procedure. **F,** Schematic of the dCas9-Dnmt3a system to allow site-specific *de novo* methylation at *RUNX1* P2 promoter. **G,** Bisulfite DNA sequencing of RUNX1 P2 promoter region upon transduction of a P2 promoter sgRNA compared with sgRNA control in MOLM-13 dCas9-Dnmt3a–expressing cells. Filled and open circles represent methylated and unmethylated CpGs, respectively. **H,** qPCR analysis of RUNX1A, RUNX1B, or RUNX1C mRNA expression in MOLM-13 dCas9-Dnmt3a cells transduced with sgRNA targeting P2 promoter from (**G**) and (**H**). Data are normalized to ACTB. *P* values were calculated using a two-tailed Student *t* test in GraphPad Prism v9.0; error bars represent SEM. *, $P < 0.05$; **, $P < 0.01$; ***, $P < 0.001$; ns, not statistically significant and performed in technical triplicates per experiment. FC, fold change; TPM, transcripts per million. (**F,** Created with BioRender.com.)

Nanopore Technologies (Oxford Nanopore Technologies) on MOLM-13 and MV4-11 cells to investigate RUNX1 isoforms. In MOLM-13 cells, which exhibit lower RUNX1C protein expression (Supplementary Fig. S2F), 51.8% of exon 2 transcripts terminated prematurely at a previously unannotated exon 3 (Supplementary Fig. S2G), which was not detected by short-read RNA-seq. This exon introduces a stop codon, generating a truncated transcript that encodes a small peptide of only 48 amino acids. These findings suggest that exon 3 may function as a putative poison exon, a type of alternative exon inclusion of which in an mRNA transcript introduces a premature termination codon. This event contributes to the significantly reduced expression of full-length RUNX1C in MOLM-13 cells. By contrast, MV4-11 cells, which express higher levels of RUNX1C, exhibited fewer premature termination events, with only 18.2% of exon 2 transcripts terminating at exon 3 (Supplementary Fig. S2G). These findings suggest that in addition to alternative promoter usage of RUNX1 isoforms, inclusion of poison exons may further modulate RUNX1 isoform expression by directing specific transcripts toward nonsense-mediated decay. In AML PDX models, we also observed that PDX#1 ($TP53^{mut}$) exhibited higher RUNX1C

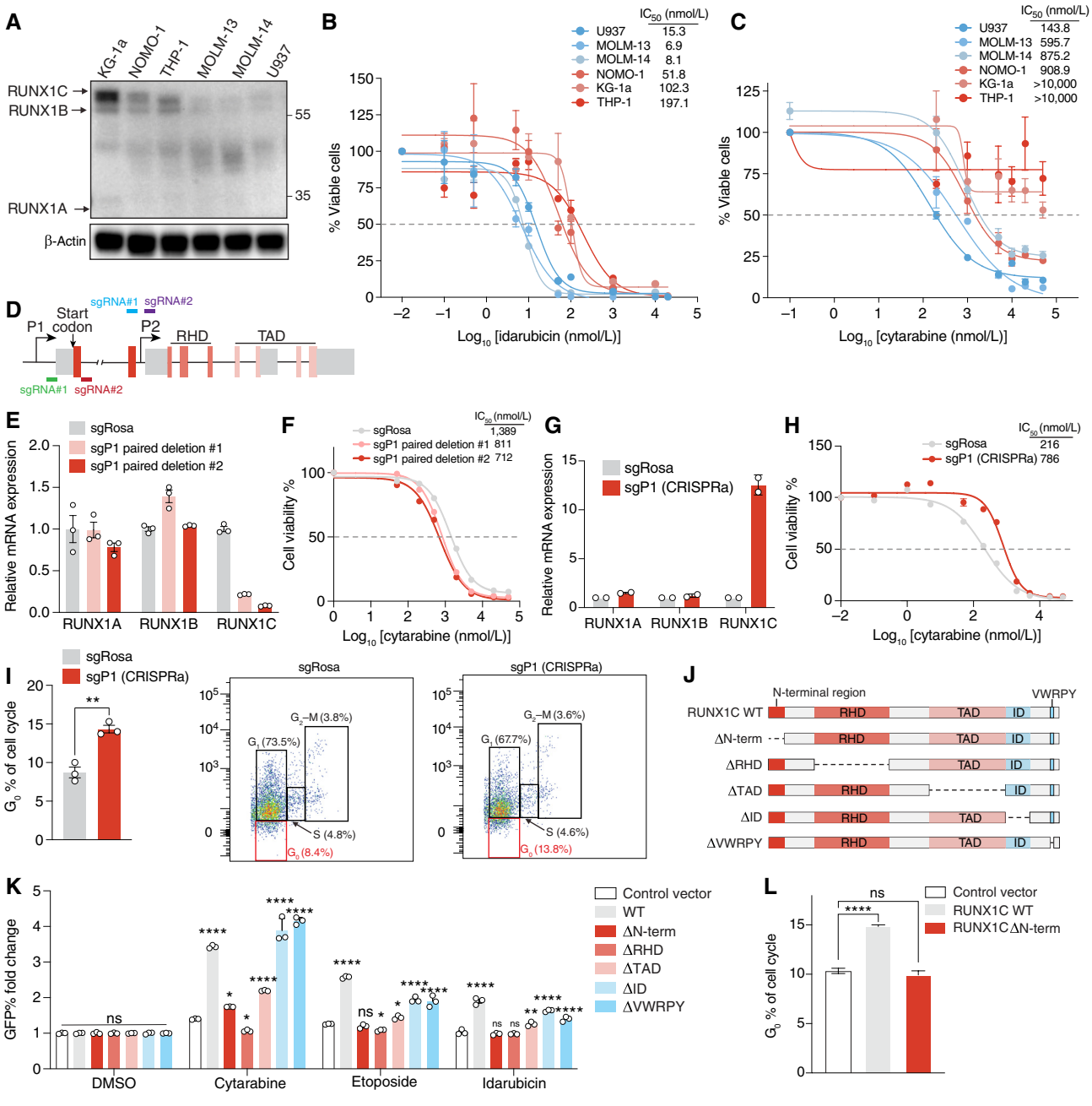

Figure 2. Long-isoform RUNX1C modulates AML chemotherapy response. **A,** Western blotting of RUNX1 protein levels in seven human AML cell lines. The long-isoform RUNX1C and RUNX1B are as indicated. **B,** Dose–response curves of human AML cell lines from (**A**) treated with various concentrations of idarubicin or (**C**) cytarabine after 48 hours. Red curves indicate AML cell lines with higher IC_{50} values (chemotherapy resistant), whereas blue curves represent cell lines with lower IC_{50} values (chemotherapy sensitive). **D,** Schematic of dual sgRNA deletion of the *RUNX1* P1 and P2 promoters. **E,** qPCR analysis of *RUNX1* isoform expression upon P1 promoter deletion in MOLM-13 cells from (**D**). Data are normalized to ACTB. #1 and #2 indicate two independent sgRNA pairs used for dual-guide deletion of the RUNX1 P1 promoter. **F,** Dose–response curves of RUNX1C dual sgRNA P1 deletion from (**E**) compared with nontargeting sgRNA (sgRosa) in MOLM-13 cells treated with various cytarabine concentrations for 48 hours. **G,** qPCR analysis of RUNX1 isoform expression upon CRISPR activation of P1 promoter of RUNX1 in MOLM-13 dCas9-VP64 and MS2-P65/HSF-1 stable cell lines. Data are normalized to ACTB. **H,** Dose–response curves of CRISPR activation of P1 promoter sgRNA compared with nontargeting sgRNA (sgRosa) in MOLM-13 from (**G**) treated with various cytarabine concentrations for 48 hours. **I,** Cell-cycle analyses by Ki-67 and DAPI upon CRISPR activation of P1 promoter sgRNA compared with sgRosa at 6 days after transduction from (**G**). Representative Ki-67/DAPI plots are shown. *P* values were calculated using a two-tailed Student *t* test. **J,** Schematic of RUNX1C cDNA protein domain mutants. **K,** Competition-based assay of MOLM-13 transduced with RUNX1C cDNA mutants from (**J**) treated with various chemotherapeutic concentrations. *P* values were calculated using one-way ANOVA. **L,** Cell-cycle analyses by Ki-67 and DAPI upon RUNX1C WT and N-terminus deletion compared with control vector at 5 days after transduction. *P* values were calculated using one-way ANOVA. All IC_{50} values were performed in technical triplicates per experiment and calculated using a nonlinear fit of log(inhibitor) vs. response (four parameters) in GraphPad Prism v9.0; error bars represent SEM. *, $P < 0.05$; **, $P < 0.01$; ****, $P < 0.0001$; ns, not statistically significant. ID, inhibitory domain; N-term, N-terminus region; RHD, Runt-homology domain; TAD, transactivation domain; VWRPY, VWRPY motif.

expression levels and greater resistance to cytarabine treatment than PDX#2 (FLT3^{ITD}, NPM1^{mut}; Supplementary Fig. S3A and S3B). In addition, we evaluated RUNX1C expression after long-term exposure to cytarabine in two independent human AML cell lines, MOLM-13 and U937, which had lower baseline RUNX1C levels and higher chemotherapy sensitivity (Fig. 2A–C). After a drug selection period of 3 weeks in the presence of cytarabine at the IC_{50} value or DMSO, we derived cytarabine-resistant (CR) cell lines, as confirmed by dose–response curves (Supplementary Fig. S3C). We found that the CR cell lines exhibited upregulated RUNX1B and RUNX1C protein expression compared with the parental cell lines (Supplementary Fig. S3D).

To functionally assess whether endogenous perturbation of *RUNX1C* levels modulates chemotherapy efficacy, we first ablated *RUNX1C* expression by using Clustered Regularly Interspaced Short Palindromic Repeats (CRISPR) to simultaneously deliver two sgRNAs to excise the intervening DNA sequence between the ATG start codon and the first coding exon of *RUNX1C* (referred to as sgP1 paired deletion and is denoted by the corresponding sgRNA pair number; Fig. 2D; Supplementary Fig. S3E; Supplementary Fig. S2C). We confirmed an approximately fourfold downregulation of *RUNX1C* levels without affecting the expression of RUNX1A/B isoforms, which led AML cells to become more sensitized to cytarabine treatment than the nontargeting control (sgRosa; Fig. 2E and F). Alternatively, CRISPR-mediated deletion of the P2 promoter that led to decreased *RUNX1B* expression did not result in differences in cytarabine response when compared with sgRosa control (Fig. 2D; Supplementary Fig. S2F–S2H). Conversely, we used the CRISPR activation (CRISPRa) system using the MOLM-13 isogenic cell line stably expressing dCas9-VP64 and p65-HSF1 with sgRNA upstream of the P1 distal promoter of RUNX1 to endogenously upregulate *RUNX1C* (referred to as P1 CRISPRa sgRNA), resulting in a 12-fold increase in *RUNX1C* expression (Fig. 2G; Supplementary Fig. S2C). We observed that CRISPRa-mediated upregulation of *RUNX1C* led to an approximately fourfold increase in the IC_{50} dose compared with the nontargeting sgRNA (Fig. 2H). Relapse can often be caused in part by residual leukemia cells that enter a reversible quiescent state to confer resistance to chemotherapy (26, 27). Previous studies have indicated that RUNX1 and certain isoforms facilitate cellular quiescence during early blood development and hair follicle stem cells (15, 28, 29); however, RUNX1 isoforms have not been studied in the context of drug resistance, to the best of our knowledge. Indeed, we observed that the endogenous upregulation of *RUNX1C* led to a significant increase in G_0 quiescent cells, as determined by Ki-67^{neg} and DAPI^{neg} staining—a widely used method for identifying quiescent cell populations (Fig. 2I; refs. 30–32). These findings underscore the importance of RUNX1C isoform expression to modulate chemotherapy response in AML.

The N-Terminus Region Is Required for RUNX1C-Mediated Chemoresistance

To characterize the protein domains of RUNX1C required for conferring chemoresistance, we performed ectopic overexpression of RUNX1C wild-type (WT) or cDNAs harboring truncations of different protein domains coupled to a GFP reporter (Fig. 2J; Supplementary Fig. S3I). Consistent with the above findings, ectopic overexpression of RUNX1C WT potently imposed a survival advantage upon treatment with various chemotherapeutic agents when compared with the DMSO control using competition-based proliferation assays (Fig. 2K). However, overexpression of RUNX1C cDNAs lacking its C-terminus regions, inhibitory domain, or VWRPY motif showed similar results as RUNX1C WT, indicating that these domains are not essential for modulating cytarabine response. As expected, the deletion of the Runt-homology domain or transactivation domain, both of which mediate DNA binding, led to diminished CR (Fig. 2K).

RUNX1 isoforms are transcribed from two alternative promoters that result in different N-termini domains (20). Human RUNX1C is the longest isoform and harbors a unique 32 amino acid at its N-terminus that is not present in other RUNX1 splice variants (33). Notably, we observed that the removal of the 32 amino acid N-terminus region of RUNX1C (ΔN-term) restored cytarabine sensitivity to levels of the control vector, which was replicated in multiple human AML cell lines (U937 and MOLM-14; Fig. 2L; Supplementary Fig. S3J and S3K). We showed that endogenous upregulation of *RUNX1C* promoted the entry of AML cells into a quiescent state (Fig. 2I). The N-terminus of RUNX1C has previously been shown to inhibit B-cell growth (33), which led us to hypothesize that this region may regulate leukemia quiescence. Consistent with our hypothesis, ectopic overexpression of RUNX1C WT significantly retained AML cells in G_0 quiescence, although the N-terminal deletion reduced quiescent AML cells (Fig. 2L; Supplementary Fig. S3L).

RUNX1/AML1 is translocated with the transcriptional repressor *ETO* gene in approximately 12% to 15% of all patients with AML and typically exhibits higher response rates to combination chemotherapy (34, 35). Interestingly, patients with *AML1-ETO* fusion lacked the unique N-terminal region of RUNX1C, which led us to reason for its enhanced efficacy to chemotherapeutic agents. As a proof-of-concept, we introduced the unique 32 amino acid N-terminus sequence of RUNX1C (referred to as RUNX1C-ETO) into the naturally occurring RUNX1-ETO translocation (Supplementary Fig. S3M). Using competition-based proliferation assays, ectopic expression of RUNX1C-ETO in AML cells showed elevated CR and etoposide treatment when compared with RUNX1-ETO (Supplementary Fig. S3N). Together, the above data revealed the biological significance of the N-terminus region of RUNX1C as a necessary regulatory domain in regulating a quiescent state and chemotherapy resistance.

Genome-Wide Binding Profiles Reveal Distinct Isoform-Specific Targets

To address the mechanisms underlying *RUNX1C*-mediated chemoresistance, we performed bulk RNA-seq of MOLM-13 cells ectopically expressing 3×FLAG-tagged isoforms A, B, C, and ΔN-term. Overexpression of RUNX1C resulted in upregulated inflammatory gene signatures that have been linked to AML progression and poor clinical outcome (36, 37), including IFN response genes (*IFITM1*, *IFITM2*, *IFITM3*, *IFI30*, *CD74*, *IRF8*, *MTHFD2*, and *IRF2BP2*), S100 alarmins (S100A4,

S100A6, S100A8, S100A9, S100A10, and S100A11), and matrix metalloproteinases (MMP9 and MMP14; Fig. 3A; Supplementary Table S2). Notably, RUNX1C overexpression did not change the expression of ATP-binding cassette (ABC) transporter genes *ABCC1*, *ABCG2*, and *ABCB1*, which have been previously implicated in cancer multidrug resistance (Supplementary Table S2; refs. 38, 39).

Given the established biochemical functioning of RUNX1 as a TF, we carried out Cleavage Under Targets and Release Using Nuclease (CUT&RUN; ref. 40) by expressing FLAG-tagged fused RUNX1-isoform cDNAs (A, B, C, and ΔN-term) in MOLM-13 cells to characterize the genome-wide binding sites of the isoform variants. CUT&RUN analysis showed significantly more peaks bound by RUNX1C (2,944), followed by RUNX1B (971) and RUNX1A (168), which predominantly occupied the intergenic, intronic, and promoter regions as previously reported (Fig. 3B; Supplementary Table S3; ref. 41). We also found that RUNX1B and RUNX1C are located near the transcriptional start site of *PU.1/SPI1*, a previously characterized direct downstream target of RUNX1 (Supplementary Fig. S4A; ref. 42). We searched for known motifs enriched within the preferential binding sites of each RUNX1 isoform using MEME-ChIP (43), which showed enrichment of the canonical Runx1 target motif (TGTGGT), further confirming our CUT & RUN method (Fig. 3C; Supplementary Fig. S4B). In total, we identified 2,485 genes that were preferentially bound by RUNX1C compared with RUNX1A or RUNX1B (Fig. 3D).

Our data showed that the N-terminal region of RUNX1C is required for AML chemosensitivity (Fig. 2K and L; Supplementary Fig. S3M and S3N), which has not been well studied. It has been previously described that the N-terminal domain alters the DNA-binding affinity of RUNX1 (44). Therefore, we speculated that this region may affect RUNX1 binding to target genes that mediate AML chemoresistance. We performed a combination of CUT&RUN and RNA-seq to characterize the gene regulatory program directly regulated by the N-terminus region of RUNX1C. Our CUT&RUN analysis identified 232 differential peaks upon deletion of the N-terminal sequence compared with RUNX1C WT. Among these regions, 142 and 90 peaks were gained or lost, respectively, in the N-terminal deletion, suggesting a dual function as negative and positive regulators of DNA binding (Fig. 3E). Together, these findings highlight an RUNX1C-mediated transcriptional program regulated by the N-terminal domain of RUNX1C.

BTG2 Is an Isoform-Specific Target that Confers Chemotherapy Resistance

To identify the direct targets of RUNX1C that mediate AML chemoresistance and quiescence, we overlapped the (i) top 50 most significantly upregulated genes in RUNX1C overexpression, (ii) CUT&RUN peaks that were preferentially bound by RUNX1C WT over RUNX1A and RUNX1B, and (iii) peaks that were lost upon deletion of the N-terminus region. Among these genes, B-cell translocation gene 2 (*BTG2*) met all these criteria as a *bona fide* transcriptional target of RUNX1C and is regulated by its N-terminal region (Fig. 4A and B). Consistent with our findings, CRISPRa-mediated upregulation of *RUNX1C* led to an increase in *BTG2* mRNA levels (Fig. 4C). To functionally assess whether RUNX1C binding at the *BTG2* promoter regulates its expression, we took advantage of protospacer adjacent motif sites to precisely mutate two separate RUNX1 core consensus motif sequences (TGTGG) located within 1 kb upstream of the *BTG2* transcription start site (referred to as the sgBTG2 RUNX1 motif; Supplementary Fig. S5A and S5B). Delivering sgRNA targeting the RUNX1 consensus sequences led to a two- to threefold downregulation of *BTG2* expression compared with nontargeting sgRNA in two independent human AML cell lines, NOMO-1 and THP-1 (Fig. 4D; Supplementary Fig. S5C).

To address the clinical relevance of our findings, we analyzed publicly available data from BeatAML, a large cohort of patients with AML subjected to *ex vivo* drug sensitivity assays (45). This analysis revealed that higher *BTG2* mRNA levels were modestly but significantly correlated with a poor response to cytarabine treatment ($r = 0.23$; Fig. 4E). Leukemia cells can enter a transient and reversible state of quiescence to allow therapeutic escape while maintaining the ability to reenter the cell cycle to resume active proliferation upon the removal of the drug (6, 46, 47). Our previous data showed that upregulated *RUNX1C* levels induce an AML quiescent state (Fig. 2I and L; Supplementary Fig. S3L). In the literature, BTG1 and BTG2 have been implicated to negatively impact proliferation (48) and promote quiescence in T cells (30). Therefore, we tested whether *BTG2* overexpression promotes AML cellular quiescence and mediates chemotherapy resistance. Here, we ectopically overexpressed BTG2 cDNA in the human AML cell lines MOLM-13 and MV4-11, which showed a twofold increase in G_0 cells compared with the control vector (Fig. 4F; Supplementary Fig. S5D). To functionally evaluate whether BTG2 levels mediate response to chemotherapy agents, we performed competition-based growth assays in multiple human AML cell lines overexpressing BTG2 and treated them with the chemotherapeutic agents, etoposide and cytarabine. Indeed, we observed that BTG2 overexpression significantly mediated broad resistance to all tested AML cell lines and chemotherapeutic agents (Fig. 4G). As *BTG2* is upregulated during myeloid maturation (49), we confirmed that its overexpression did not induce AML differentiation (Supplementary Fig. S5E), which indicates that our results can be attributed to cellular quiescence. Importantly, ablation of BTG2 enhanced cytarabine efficacy compared with control sgRNA (Fig. 4H). Based on these results, we questioned whether targeting BTG2 could promote AML cells to exit quiescence and become sensitized to chemotherapy. Ablation of BTG2 in AML cells led to exit from the G_0 quiescent program and cell-cycle reentry into G_1 when compared with the nontargeting sgRNA control (Fig. 4I). Furthermore, we performed a cell viability assay by overexpressing RUNX1C in BTG2-deficient or BTG2-intact (nontargeting sgRNA) AML cells (Supplementary Fig. S5F). We observed that BTG2 deficiency attenuated the chemotherapy resistance of RUNX1C-overexpressing MOLM-13 AML cells (Supplementary Fig. S5F). To determine whether BTG2 induction results from cell quiescence or is directly mediated by RUNX1C, we performed ectopic overexpression experiments in MOLM-13 cells transduced with either an RUNX1C overexpressing or control vector, followed by high-dose cytarabine or DMSO treatment. In control vector–transduced cells, cytarabine induced about fourfold increase in BTG2 expression compared with DMSO, suggesting an RUNX1C-independent effect. However, in

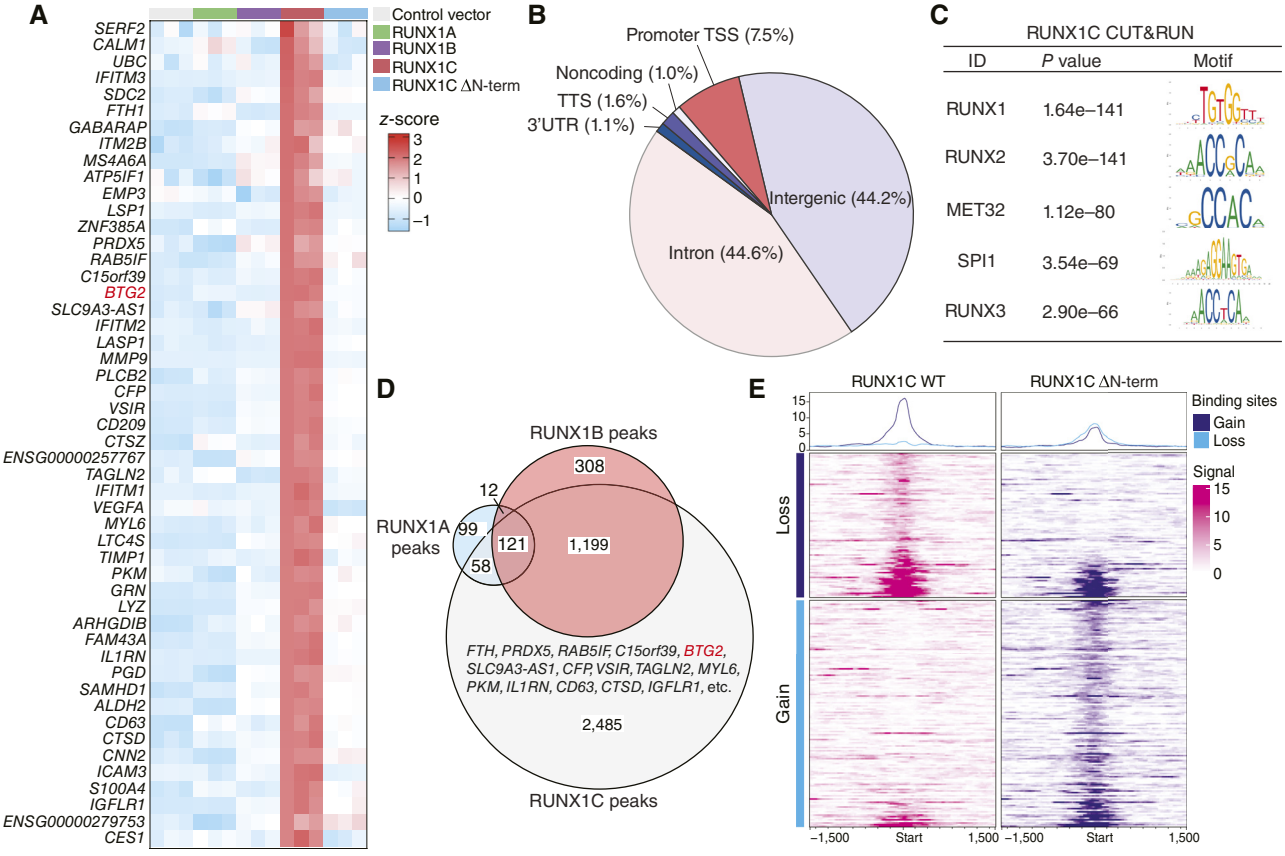

Figure 3. Genome-wide binding profiles reveal differential targets regulated by RUNX1C. **A,** Heatmap of top differential genes expressed in MOLM-13 cells transduced with RUNX1 cDNA splice variants and RUNX1C N-terminus deletion. **B,** Genomic binding distribution of RUNX1C CUT&RUN in MOLM-13 cells. **C,** RUNX1C CUT&RUN *de novo* motif analysis in MOLM-13 cells using MEME-ChIP software. Statistical analysis was calculated using the binomial test. **D,** Venn diagram of differential genes bound by RUNX1 isoforms. **E,** Metaplot of *z*-scores representing binding sites and surrounding 1.5 kb upstream and downstream in RUNX1C WT and RUNX1C N-terminus deletion. All data were generated as biological triplicates. TSS, transcriptional start site; UTR, untranslated region.

RUNX1C-overexpressing cells treated with cytarabine, BTG2 expression increased dramatically (about 12-fold), supporting a role for RUNX1C in BTG2 induction (Supplementary Fig. S5G). Taken together, these findings demonstrate that BTG2 is a direct target of RUNX1C that mediates AML quiescence and chemoresistance.

BTG2-Mediated Deadenylation of Ribosomal RNAs Promotes AML Quiescence

BTG2 interacts with the deadenylation complex to reduce poly(A) tails and mRNA stability (50, 51). To this end, we implemented direct native LR-seq (52) to characterize the genome-wide 3′ poly(A) tail length changes in mRNA transcripts. Consistent with its known role in mRNA destabilization (50, 53), we observed that ectopic overexpression of BTG2 led to a significant global shortening of poly(A) tail lengths (74 nucleotides) compared with the control vector (77 nucleotides; Fig. 5A; Supplementary Table S4). Interestingly, Gene Ontology analysis showed that "large and small ribosomal subunits" were the most significantly enriched terms among deadenylated transcripts in BTG2 overexpression (Fig. 5B and C). It has been suggested that shorter poly(A) tail length on mRNAs is translated less efficiently and is associated with abundantly expressed genes (e.g., ribosomal proteins; refs. 54, 55). Moreover, hematopoietic stem cells that undergo quiescence have reduced protein synthesis rates compared with cycling hematopoietic progenitors (56–58). Based on these studies, we hypothesized that BTG2 overexpression alters mRNA stability of ribosomal proteins to diminish protein translation and promote a quiescence state.

To assess the role of BTG2 in protein translation, we implemented O-propargyl–puromycin (OP-Puro) incorporation assays to fluorescently label and measure protein synthesis using flow cytometry (56). Ectopic overexpression of BTG2 resulted in significantly less incorporation of OP-Puro, indicating a global reduction in protein synthesis (Fig. 5D; Supplementary Fig. S6A). As shorter poly(A) tail lengths may act to reduce mRNA stability, we assessed the decay of rRNAs at multiple timepoints after actinomycin D treatment in MOLM-13 cells ectopically expressing BTG2 or the control vector. RT-qPCR of large (RPL19 and RPL13A) and small (RPS11, RPS10, RPS9, RPS6, RPS27A, and RPS19) rRNAs showed significantly increased mRNA decay in BTG2 overexpression compared with that in the control vector (Fig. 5E). As negative controls, we measured the transcript decay of genes that did not exhibit shorter poly(A) tails upon BTG2

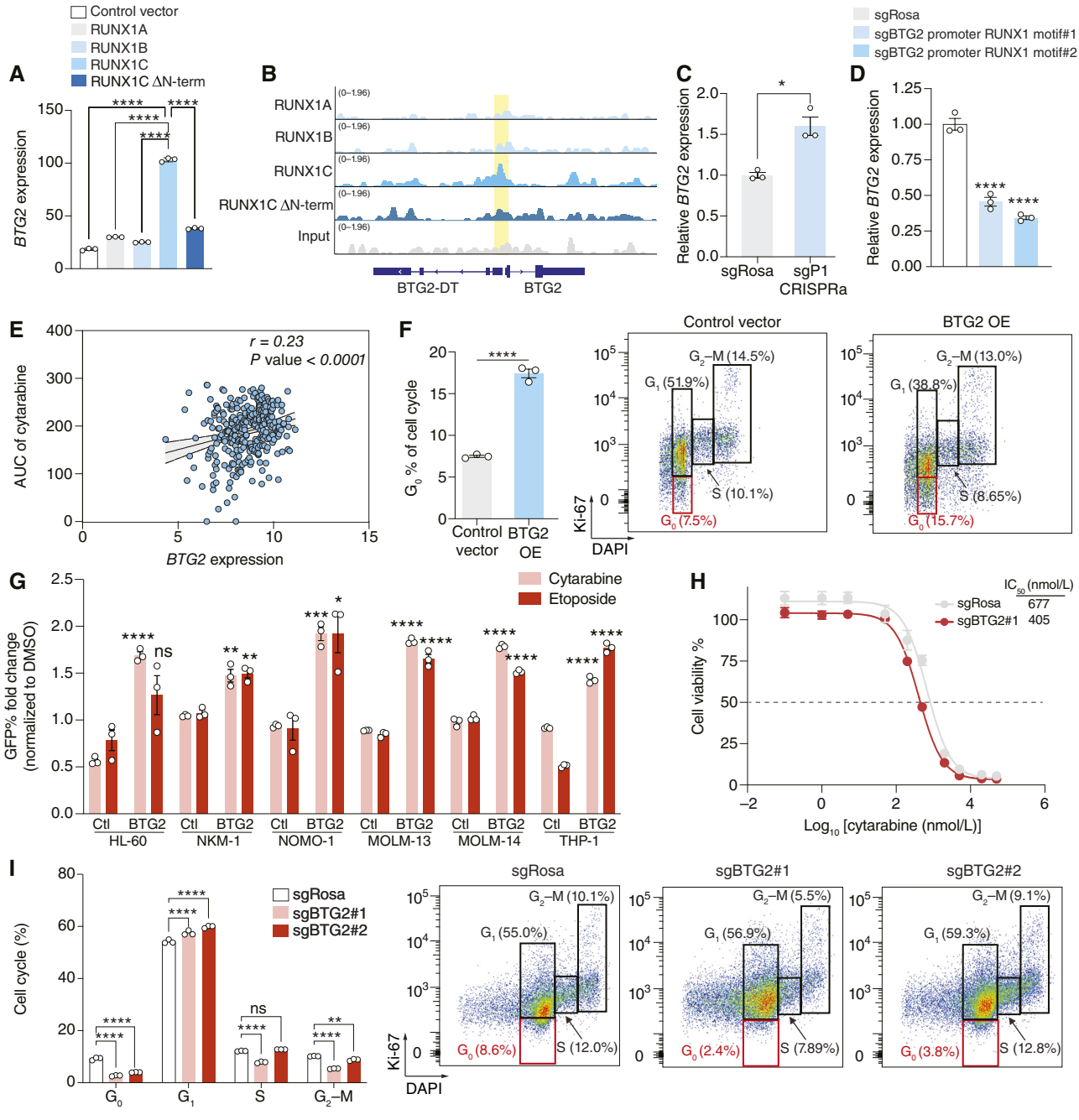

Figure 4. BTG2 promotes AML chemoresistance. **A,** *BTG2* expression of fragments per kilobase of transcript per million fragment mapped (FPKM) from RUNX1 cDNA isoforms from RNA-seq in MOLM-13 cells. **B,** RUNX1 isoform binding at *BTG2* gene. Spike-in-normalized signals are used in CUT&RUN tracks. **C,** qPCR analysis of *BTG2* expression upon CRISPR activation of *RUNX1C* in MOLM-13 dCas9-VP64 and MS2-P65/HSF-1 stable cell lines. Data are normalized to ACTB. *P* values were calculated using a two-tailed Student *t* test. **D,** qPCR analysis of sgRNA targeting RUNX1 motif sequences nearby *BTG2* transcription start site in NOMO-1 cells. **E,** Pearson correlation plot for *BTG2* expression in patients with AML from BeatAML database. Each dot represents a sample from an individual with AML ($n = 301$). **F,** Cell-cycle analyses by Ki-67 and DAPI of BTG2 overexpression compared with control vector in MOLM-13 AML cells 4 days after transduction. Representative Ki-67/DAPI plots are shown. *P* values were calculated using a two-tailed Student *t* test. **G,** Competition-based assay of six human AML cell lines transduced with BTG2 cDNA or control vector and treated with cytarabine, etoposide, or DMSO control. *P* values were calculated using one-way ANOVA. **H,** Dose–response curves of BTG2 knockout in MOLM-13 AML cells treated with various cytarabine concentrations after 48 hours. **I,** Cell-cycle analyses by Ki-67 and DAPI of BTG2 sgRNAs compared with sgRosa in MOLM-13 AML cells 6 days after transduction. Representative Ki-67/DAPI plots are shown. All error bars represent SEM. *, $P < 0.05$; **, $P < 0.01$; ***, $P < 0.001$; ****, $P < 0.0001$; ns, not significant. OE, overexpression.

overexpression (Supplementary Fig. S6B). Among these ribosomal genes, RPL5 and RPL17 showed elevated mRNA levels and reduced protein levels upon BTG2 overexpression (Fig. 5F).

Next, we developed a lentiviral cell-cycle reporter using a previously described p27 inactive mutant (p27K) that prevents CDK binding (59), fused to mCherry, to quantitatively

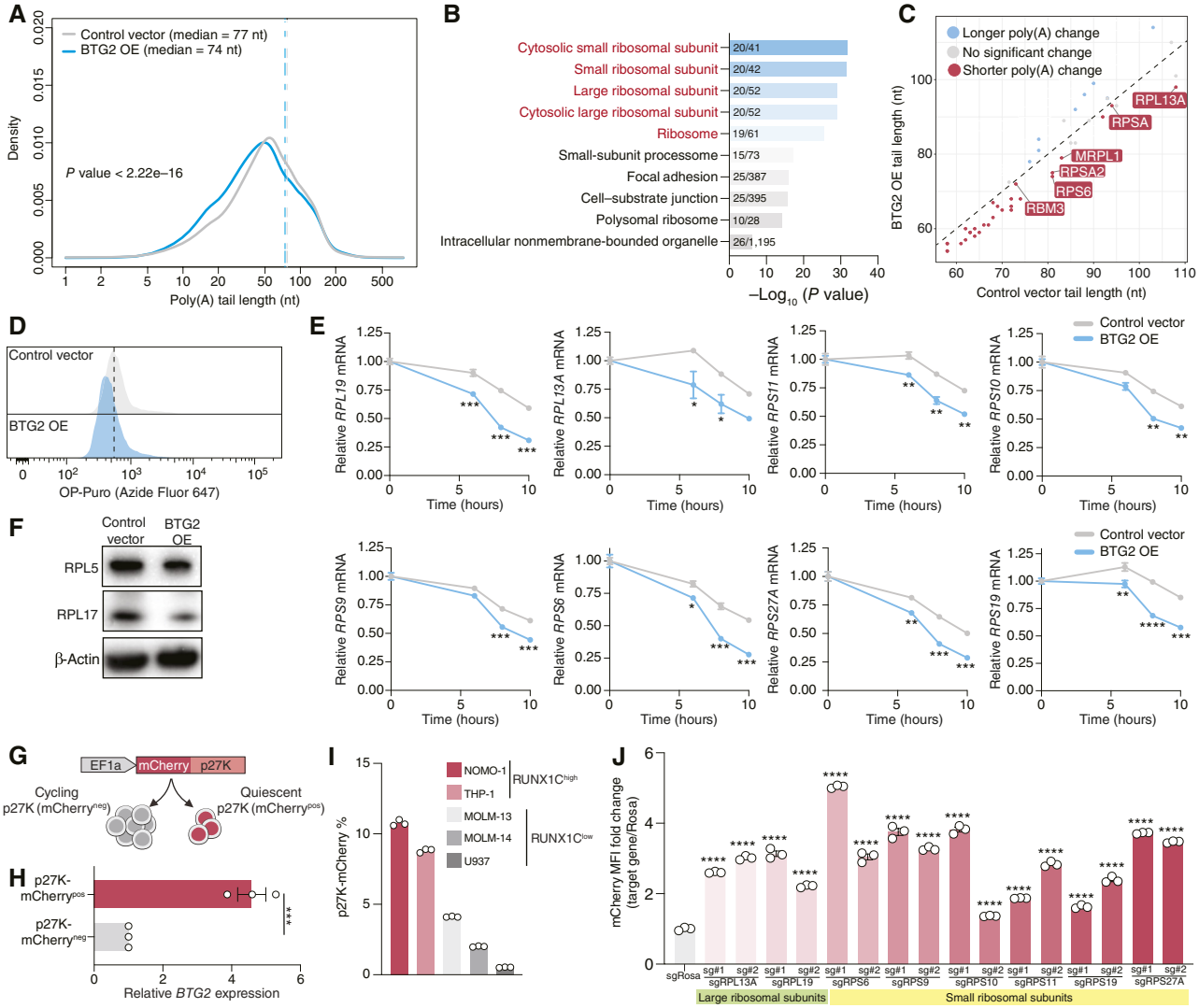

Figure 5. BTG2-mediated deadenylation of rRNAs promotes AML quiescence. **A,** Distribution of poly(A) tail lengths based on direct LR-seq upon BTG2 cDNA overexpression compared with control vector in MOLM-13 cells 4 days after transduction. Median tail lengths are as indicated. **B,** Gene Ontology enrichment analysis of terms enriched in shorter poly(A) tail lengths upon BTG2 overexpression compared with control vector. **C,** Scatter plot of poly(A) tail lengths upon BTG2 overexpression compared with control vector. Plotted are GO terms associated with ribosomal genes from (**B**). **D,** Representative flow cytometry plots of OP-Puro incorporation assays in BTG2 overexpression compared with control vector 4 days after transduction in MOLM-13 cells. **E,** qPCR analysis of ribosomal transcripts in BTG2 overexpression at multiple timepoints after actinomycin D (2.5 μg/mL) treatment. **F,** Western blotting of ribosomal proteins RPL5 and RPL17 in MOLM-13 cell overexpressing BTG2 or control vector. β-Actin was used as the loading control. **G,** Schematic of p27K-mCherry lentiviral reporter system. **H,** qPCR analysis of *BTG2* expression in MOLM-13 cells sorted on quiescent cells (p27K-mCherry^{pos}) or cycling (p27K-mCherry^{neg}) MOLM-13 cells. **I,** Flow cytometric analysis of p27K-mCherry expression in five human AML cell lines. **J,** Flow cytometric analysis of p27K-mCherry median fluorescence intensity (MFI) expression upon CRISPR-mediated deletion of large and small ribosomal subunits in MOLM-13 AML cells 6 days after transduction. All error bars represent SEM. *P* values were calculated using one-way ANOVA. *, $P < 0.05$; **, $P < 0.01$; ***, $P < 0.001$; ****, $P < 0.0001$. nt, nucleotide; OE, overexpression.

measure the population of live G_0 quiescent cells across human AML cell lines (Fig. 5G). We further confirmed that mCherry^{high}-p27K quiescent AML cells exhibited an approximately fourfold increase in *BTG2* expression, as well as other quiescent gene signatures, compared with cycling cells (mCherry^{neg}-p27K; Fig. 5H; Supplementary Fig. S6C). Notably, AML cell lines that we previously showed had RUNX1C^{high} protein expression (THP-1 and NOMO) exhibited higher baseline expression of mCherry-p27K quiescent cells than RUNX1C^{low} AML cell lines (MOLM-13, U937, and MOLM-14; Fig. 5I; Supplementary Fig. S6D). Moreover, MOLM-13 cells treated with increasing doses of cytarabine showed higher mCherry-p27K expression (Supplementary Fig. S6E). Despite the overall small percentage of quiescent cells (mCherry-p27K), mCherry^{high}-p27K–sorted cells exhibited greater resistance to high-dose cytarabine than mCherry^{low}-p27K–sorted cells (Supplementary Fig. S6F). Consistent with previous studies (56, 57), mCherry^{high}-p27K quiescent cells exhibited significantly less incorporation of OP-Puro and thus lower global protein synthesis than mCherry^{neg}-p27K

cycling cells (Supplementary Fig. S6G). Next, we used our p27K lentiviral reporter system to assess the quiescent population upon CRISPR-mediated perturbation of the large or small ribosomal subunits. Our results showed that CRISPR-mediated ablation of large and small ribosomal genes led to a significant increase in the mCherry-p27K quiescent population relative to nontargeting sgRosa (Fig. 5J; Supplementary Fig. S6H and S6I). These data support a model in which BTG2 deadenylates rRNAs to lower protein synthesis rates and promotes AML quiescence. To our understanding, this has not been previously described.

RNA Targeting of RUNX1C Improves Chemotherapeutic Efficacy *In Vitro* and *In Vivo*

Next, we assessed the feasibility of targeting *RUNX1C* mRNA to enhance chemotherapy efficacy by eradicating treatment-resistant cancer cells. Previous studies have shown that RUNX1 is crucial for blood cells (12); however, it is dispensable for adult hematopoiesis (13, 60). Notably, the genetic deletion of *RUNX1C* has no impact on normal adult hematopoiesis (23). Together, these studies present a therapeutic opportunity to target the *RUNX1C* splice variant to potentiate chemotherapy response. The discovery of Cas13 proteins has enabled RNA knockdown in mammalian cells with minimal off-target effects (61). To assess whether Cas13-mediated RNA targeting of *RUNX1C* mRNA can increase chemosensitivity, we generated a human MOLM-13 AML cell line stably expressing Cas13 driven by a tetracycline-inducible promoter (61) that we confirmed upon doxycycline treatment (Fig. 6A; Supplementary Fig. S7A). In parallel, we designed isoform-specific sgRNAs against the first two exons of the *RUNX1C* transcript (referred to as sgRUNX1C Cas13), which are not present in the other RUNX1 isoforms (Supplementary Fig. S2C; Supplementary Table S5). We measured levels of all three isoforms at the mRNA and protein levels in cells with control versus Cas13-mediated knockdown of *RUNX1C* mRNA (Fig. 6B; Supplementary Fig. S7B).

By using Ki-67 staining, we observed that Cas13 targeting of *RUNX1C* led to increased G_0 to G_1 transition (Supplementary Fig. S7C). Next, we assessed the combination of RUNX1C knockdown and cytarabine treatment in AML cells. Notably, we demonstrated that RUNX1C inhibition enhanced cytarabine treatment of MOLM-13 AML cells (Fig. 6C). In addition, this was also observed in an intrinsically chemotherapy-resistant TP53-mutated AML cell line, THP-1, which showed that Cas13 targeting of *RUNX1C* significantly conferred cytarabine sensitivity (Fig. 6D). Given the potential for Cas13 to induce collateral activity based on previous literature (62), we sought to validate our results using an orthogonal RNA-targeting system. Here, we introduced a tetracycline-inducible short hairpin RNA (shRNA) targeting *RUNX1C* and confirmed its knockdown in MOLM-13 cells (Supplementary Fig. S7D). In agreement with our findings, shRNA-mediated knockdown of *RUNX1C* in AML cells also increased G_0 to G_1 transition and sensitivity of AML cells to cytarabine compared with the nontargeting shRNA control (Supplementary Fig. S7E–S7G). Given that RUNX1 has been previously implicated in AML growth (63), we investigated its impact to delineate the specific contributions of its isoforms. We designed sgRNAs targeting all annotated RUNX1 isoforms (pan-RUNX1 sgRNA), which led to reduced AML survival (Supplementary Figs. S2C, S7H, and S7I), consistent with previous findings (63). However, we observed that pan-RUNX1 deletion did not induce chemosensitivity as observed with RUNX1C-specific ablation (Supplementary Fig. S7J). These data suggest that chemosensitivity depends on selective RUNX1C targeting and results in an RUNX1A/B isoform shift, whereas pan-RUNX1 deletion may disrupt this critical balance and abrogate drug response.

We next assessed the *in vivo* efficacy of Cas13-mediated degradation of RUNX1C mRNA in AML progression by transplanting MOLM-13 AML cells expressing firefly luciferase into immunodeficient recipient mice. To resemble the disease burden in patients, we waited until the onset of disease, as confirmed by using bioluminescent imaging, followed by induction of Cas13 expression by doxycycline administration and cytarabine treatment (60 mg/kg per day; Fig. 6E). In agreement with the *in vitro* findings, bioluminescent quantification and imaging of animals with Cas13 targeting of *RUNX1C* mRNA and treatment with cytarabine showed a marked delay in AML burden *in vivo* (Fig. 6E and F). Importantly, Cas13-mediated knockdown of RUNX1C extended survival in the setting of cytarabine treatment compared with the vehicle control and nontargeting sgRNA (Fig. 6G).

To assess the translational potential of this work, we designed antisense oligonucleotides (ASO) targeting *RUNX1C* mRNA used 2′-O-methoxyethyl phosphorothioate chemistry for increased ASO stability and fewer off-target effects. Our data showed that ASO treatment resulted in an approximately fourfold downregulation of *RUNX1C* mRNA in AML PDX ($FLT3^{ITD}$ and $NPM1^{mut}$) cells compared with control ASO after 4 days of treatment (Supplementary Fig. S7K). Notably, ASO-mediated knockdown of *RUNX1C* mRNA in PDX cells exhibited increased antileukemic effects compared with control ASO when combined with cytarabine treatment (Fig. 6H and I). Together, these findings highlight the therapeutic potential of targeting *RUNX1C* isoform to potentiate chemotherapy efficacy in AML, suggesting a potential therapeutic approach for patients.

DISCUSSION

Despite our current understanding of mRNA isoforms in leukemogenesis, the impact of RNA isoforms on disease relapse remains unclear. To address this challenge, we conducted a comprehensive analysis characterizing the AS landscape of patients at pretreatment and at relapse after chemotherapy. These data, combined with bisulfite sequencing, revealed epigenetic dysregulation of alternative promoters that alter RUNX1 isoform–specific expression at relapse after chemotherapy. We further demonstrated that genetic perturbation of RUNX1C expression is pivotal for modulating the response to chemotherapeutic agents in AML. TF isoforms of genes such as RUNX1 are often differentially expressed and exhibit distinct cellular functions that can promote cancer cell survival (64, 65). Despite extensive studies on the role of RUNX1 in early blood development and leukemogenesis, wherein it is frequently mutated, its isoform-dependent functions in drug resistance are not well understood. The Runt-homology

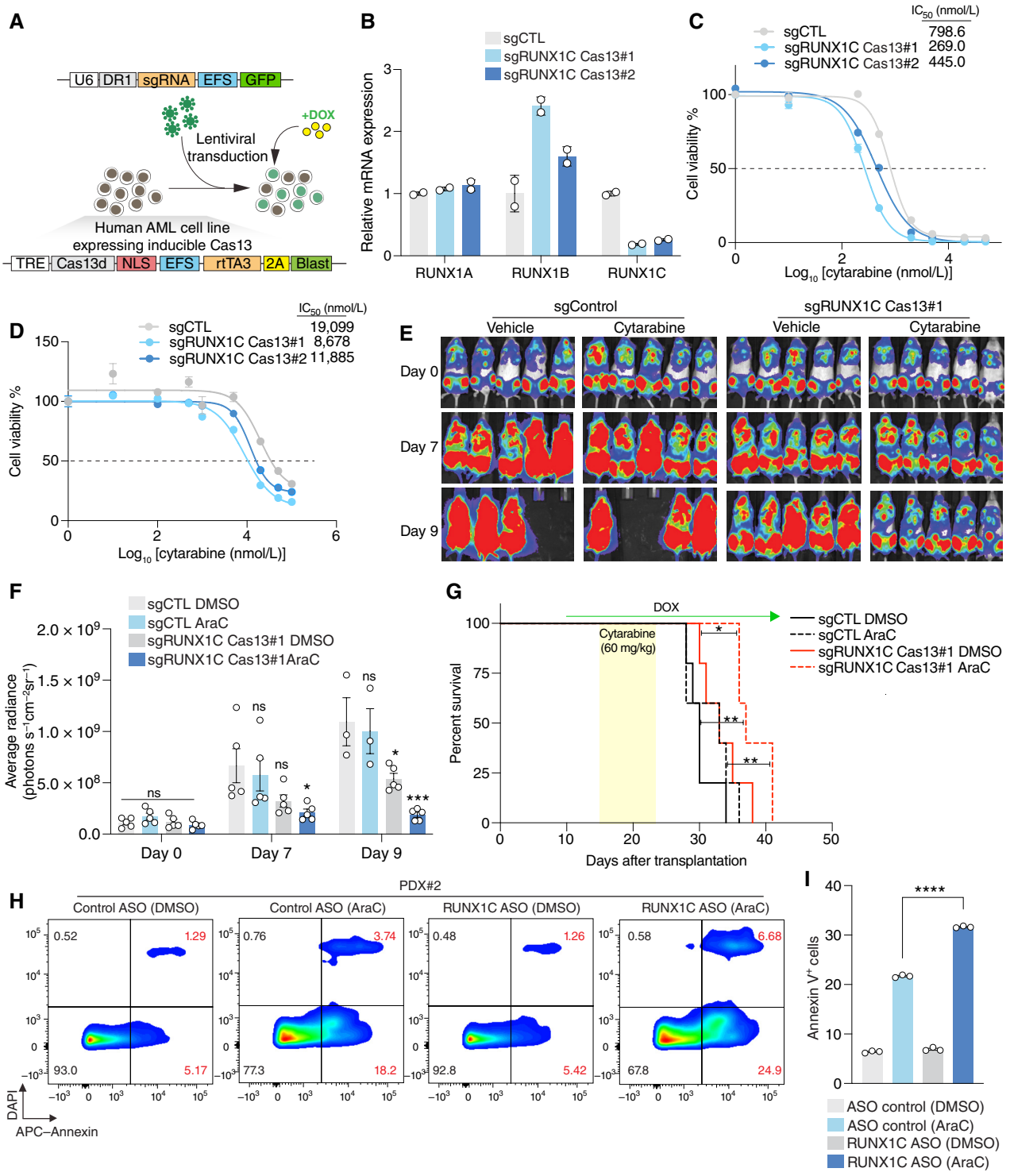

Figure 6. RNA targeting of RUNX1C enhances chemosensitivity. **A,** Schematic of the two-component inducible Cas13 (CasRfx) system in human AML cell lines. **B,** qPCR analysis of RUNX1 isoform expression treated with doxycycline for 4 days in MOLM-13 cells. Error bars represent technical triplicates. **C,** Dose–response curves of MOLM-13 or (**D**) THP-1 AML cells transduced with RUNX1C sgRNAs and treated with various cytarabine (AraC) concentrations. **E,** Bioluminescent images of mice transplanted with MOLM-13 cells transduced with sgControl (sgCTL) or sgRUNX1C and treated with vehicle or cytarabine (AraC) (60 mg/kg). The same mice are depicted at each timepoint. **F,** Quantification of bioluminescent imaging and (**G**) Kaplan–Meier survival curves of mice in (**E**). The *P* values were determined using the log-rank Mantel–Cox test. **H,** Representative flow cytometry plots of annexin V staining performed on PDX#2 ($FLT3^{ITD}$ and $NPM1^{mut}$) cells treated with 500 nmol/L RUNX1C ASO or control ASO for 4 days and DMSO or cytarabine (AraC) (500 nmol/L) for 2 days. **I,** Quantification of annexin-positive cells from (**H**). IC_{50} values are calculated from at least three technical replicates per experiment. All error bars represent SEM. All IC_{50} values were performed in technical triplicates per experiment and calculated using a nonlinear fit of log(inhibitor) vs. response (four parameters) in GraphPad Prism v9.0; error bars represent SEM. *, $P < 0.05$; **, $P < 0.01$; ***, $P < 0.001$ ****, $P < 0.0001$; ns, not significant.

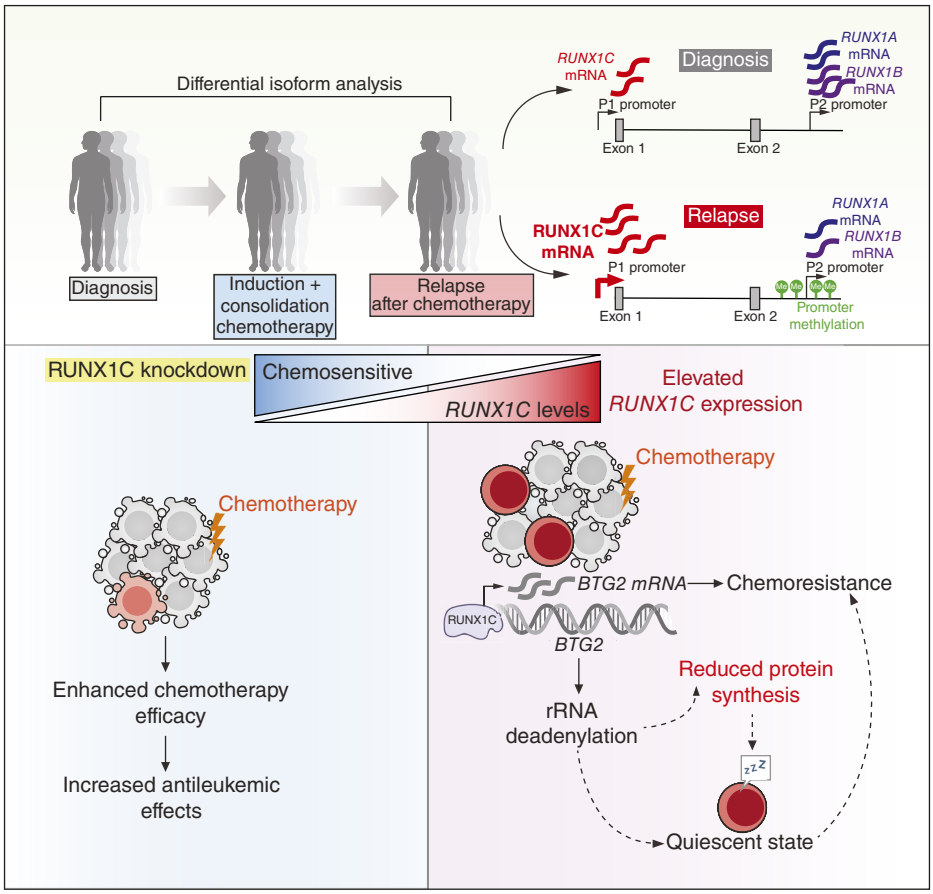

Figure 7. Schematic model of RUNX1C isoform regulating BTG2 expression to promote AML quiescence and chemoresistance. **Top**, Differential isoform analysis of matched patient samples at diagnosis vs. at relapse after chemotherapy reveals isoform-specific changes in RUNX1. At diagnosis, transcriptome-wide isoform profiling shows lower expression of the P1-driven RUNX1C isoform (red). After induction + consolidation chemotherapy, relapsed blasts have high RUNX1C expression, coincident with increased DNA methylation at the P2 promoter (green "Me" symbols) and reduced RUNX1A/B. **Bottom**, Functional consequences of RUNX1C modulation during chemotherapy exposure. Bottom left, pharmacologic or genetic inhibition of RUNX1C sensitizes AML cells (red) to chemotherapy (lightning bolt), enhancing cell death, delaying relapse, and prolonging survival. Bottom right, elevated RUNX1C during chemotherapy drives transcriptional upregulation of BTG2, which promotes rRNA deadenylation, reduced global protein synthesis, and entry into a quiescent, chemotherapy-resistant state.

domain of RUNX1 is a *bona fide* DNA-binding domain critical for transcriptional regulation. However, the functional relevance of the different N-terminal regions encoded by RUNX1 isoforms remains unclear. In this study, we provide the first genome-wide characterization of the transcriptional program mediated by the N-terminus region of RUNX1C that drives chemotherapy resistance. We found that the N-terminal region of RUNX1C regulates a subset of RUNX1 target genes, including *BTG2* that is necessary for promoting a quiescent phenotype in AML, which was not observed in other RUNX1 splice variants. Importantly, RNA targeting of RUNX1C sensitized AML cells to chemotherapy treatment (Fig. 7).

In addition to the RUNX1C–BTG2 axis, our data suggest that there may be other mechanisms of RUNX1C-associated drug resistance. Notably, we observed a marked upregulation of IFNγ signaling pathway, including IFITM1, IFITM2, and IFITM3, upon RUNX1C overexpression. These genes have been implicated in drug resistance and poor prognosis in AML, pointing to a multifaceted role for RUNX1C in mediating chemoresistance (66, 67). This finding expands our understanding of RUNX1C's function and highlights the need for future studies to explore the contribution of these inflammatory mediators to drug resistance.

In our study, we demonstrated that genetic and chemical RNA targeting of *RUNX1C* mRNA enables AML cells to exit quiescence and enhance chemotherapy efficacy. Although advances in RNA therapeutics have allowed researchers to directly target genes that are traditionally difficult to inhibit with small molecules, their clinical application is still hampered by significant limitations. These include poor stability in biological environments and inefficient delivery of oligonucleotide-based therapies to tumor cells *in vivo*, leading to reduced efficacy and safety. Despite these hurdles, recent progress in chemical modifications of ASOs has shown potential, particularly in targeting AML cells. Previous studies have shown that Toll-like receptor 9–specific oligodeoxynucleotides containing unmethylated CpG motifs can silence genes specifically in immune cells recognized by Toll-like receptor 9, including myeloid and B cells (68). These findings highlight the feasibility of the

CpG-siRNA approach to silence genes in TLR9+ tumor cells, potentially addressing some of the traditional challenges of ASO therapy.

We identified BTG2 as a regulator of AML quiescence and chemoresistance. Although several studies have linked BTG2 to mRNA stability (30, 50, 51), its specific deadenylated mRNA targets have not been well characterized. In this study, we used native LR-seq, which revealed a previously unknown mechanism by which BTG2 regulates rRNAs through deadenylation and degradation of its transcripts. The degradation of rRNA transcripts leads to reduced global protein synthesis, a hallmark of hematopoietic stem cell quiescence (56–58). Gene promoters are often enriched for binding to multiple TFs. Our findings show that RUNX1C directly binds to and regulates *BTG2* levels. Notably, our longitudinal samples collected from patients with AML at relapse after chemotherapy, a stage with treatment pressure that is marked by leukemic repopulation, did not show any changes in *BTG2* expression as compared with that at diagnosis (Supplementary Fig. S7L). By contrast, our findings model an immediate response to chemotherapy that robustly induces BTG2 (Supplementary Fig. S5G). We hypothesize that during this acute phase, RUNX1C cooperates with TP53 (69), also known as BTG2 activator, whereas at relapse, attenuated DNA damage signaling and TP53 activity allow proliferation despite high *RUNX1C* expression, implying that additional factors are needed to induce *BTG2*. In summary, our work identifies that the RUNX1C–BTG2 axis as a critical mechanism for quiescent leukemia cells may contribute to chemotherapy resistance and RNA targeting of RUNX1C as a promising therapeutic strategy may contribute to potentially mitigate AML relapse.

METHODS

Cell Lines and Cell Culture

All human leukemia cell lines were cultured in RPMI medium with 10% FBS and 1% penicillin/streptomycin. HEK293T cells were grown in DMEM supplemented with 10% FBS and 1% penicillin/streptomycin. Cell lines transduced with lentiviral Cas9 blasticidin (Addgene, plasmid number 52962) were selected using blasticidin (Thermo Fisher Scientific) 48 hours after transduction. The CRISPRa AML isogenic cell line was generated by transducing MOLM-13 cells with a lentiviral vector encoding MS2-P65-HSF1 with a hygromycin resistance marker (lentiMPH v2; Addgene, plasmid number 89308) and dCas9-VP64 with a blasticidin resistance marker (Addgene, plasmid number 61425). The MOLM-13 dCas9-Dnmt3a cell line was generated by transducing with the Fuw-dCas9-Dnmt3a-P2A-tagBFP construct (Addgene, plasmid number 84569) and selecting isogeneic clones with high dCas9-Dnmt3a protein expression by using Western blotting. Cas13 cell lines were generated by transducing THP-1 or MOLM-13 AML cell lines with RfxCas13d expressing a TetO promoter and a blasticidin resistance marker (Addgene, plasmid number 138149). All transfections were performed in HEK293T cells using polyethylenimine reagent at 4:2:3 ratios of plasmid:pVSVG:pPax2 in Opti-MEM solution. Viral supernatants were collected 24 and 48 hours after transfection. Spin infections were performed at room temperature (1,800 RPM for 30 minutes with a polybrene reagent (1:2,000 dilution; Thermo Fisher Scientific). All cell lines were authenticated using the Arizona Genetics RII Core based on fragment and short tandem repeat analyses. All cell lines were tested for *Mycoplasma* contamination. MOLM-13 (DSMZ, Cat. #ACC554; RRID: CVCL_2119), MOLM-14 (DSMZ, Cat. #ACC777; RRID: CVCL_7916), MV4-11 (ATCC, Cat. #CRL-9591; RRID: CVCL_0064), THP-1 (ATCC, Cat. #TIB-202; RRID: CVCL_0006), NOMO-1 (DSMZ, Cat. #ACC542; RRID: CVCL_1609), U937 (ATCC, Cat. #CRL-1593.2; RRID: CVCL_0007), HEK293T (ATCC, Cat. #CRL-1573; RRID: CVCL_0063), and KG-1a (ATCC, Cat. #CCL-246.1; RRID: CVCL_1824).

AML PDXs

Primary bone marrow and blood specimens were collected from patients with leukemia and lymphoma at the Dana-Farber Cancer Institute, Brigham and Women's Hospital, and Boston Children's Hospital. De-identified patient samples were obtained with written informed consent, and the studies were conducted in accordance with recognized ethical guidelines approved by the Dana-Farber/Harvard Cancer Center Institutional Review Board–approved protocol #13-351 (70). NOD/SCID IL2Rγ mice were purchased from The Jackson Laboratory and handled according to the Dana-Farber Cancer Institute Institutional Animal Care and Use Committee–approved protocol #13-034. Targeted exon capture and next-generation sequencing of all coding exons of 205 genes are described in the article by Townsend and colleagues (70). PDXs were cultured in StemSpan Leukemia Cell Culture Medium (STEMCELL Technologies), according to the manufacturer's protocol. PDX#1 is derived from primary bone marrow AML specimens with a TP53 mutation and is described as a 48-year-old male with no prior treatments. PDX#2 is derived from primary bone marrow AML specimens with a $FLT3^{ITD}$ and $NPM1^{mut}$ and is described as a 61-year-old male patient with acute myelocytic leukemia M4/M5 that has been treated with induction therapy, consolidation high-dose cytarabine, and allogenic hematopoietic stem cell transplantation. Patient race and ethnicity were not reported.

Animal Studies

About 8- to 10-week-old NSG-SGM3 male mice were obtained from The Jackson Laboratory. The mice were bred and maintained in individual ventilated cages and fed autoclaved food and water at UConn Health. All animal experiments were performed in accordance with protocols approved by the Institutional Animal Care and Use Committee, according to national and institutional guidelines. For Cas13 expression induction, animals were treated with doxycycline in drinking water (2 mg mL^{-1} with 2% sucrose; Sigma-Aldrich) and food (625 mg kg^{-1}; Teklad). For cytarabine treatment, a stock of 50 mg mL^{-1} cytarabine in DMSO was diluted eightfold with a 10% 2-hydroxypropyl-β-cyclodextrin carrier (Sigma-Aldrich). Mice were intraperitoneally injected daily with freshly diluted cytarabine (60 mg kg^{-1}) or a similar volume of a carrier containing 10% DMSO. Kaplan–Meier survival curves were compared using the Wilcoxon rank-sum test in GraphPad Prism.

cDNA Experiments

For cDNA analysis, RUNX1A (NM_001122607.2), RUNX1B (NM_001001890.3), RUNX1C (NM_001754.5), and BTG2 (NM_006763.3) were cloned into a lentiviral vector (EF1α promoter-IRES-puromycin-T2A-Zsgreen). For all CUT&RUN and RNA-seq, RUNX1 cDNA isoforms were fused with a C-terminal 3×FLAG. All cloning procedures were performed using an In-Fusion cloning system (Clontech, #638909) and sequenced using Plasmidsaurus.

In Vitro Competition Assay

RUNX1A, *RUNX1B*, *RUNX1C*, *RUNX1C* mutants, *BTG2*, *RUNX1C-ETO*, and *RUNX1-ETO* were synthesized as gene blocks by Twist Bioscience and subcloned into a lentiviral Puro-IRES-GFP construct using the NEBuilder HiFi DNA Assembly. For the competition assay to evaluate the drug response of cDNA overexpression, cell lines were transduced with cDNAs (Puro-IRES-GFP) constructs, and the percentage of GFP-expressing cells was measured 2 days after transduction and treated with drugs for 48 hours using BD LSRFortessa.

On day 2 after transduction, AML cells were cultured in RPMI/10% FBS with cytarabine (MedChemExpress, HY-13605), etoposide (MedChemExpress), daunorubicin (Selleckchem), or idarubicin (Selleckchem). The GFP-positive rate in living cells at each time-point compared with that in DMSO was calculated.

Western Blotting

Proteins were harvested using whole-cell lysis RIPA buffer. Lysate protein concentration was measured with the BCA reagent and 10 to 30 mcg was loaded per lane onto 4% to 12% NuPAGE Bis-Tris protein gels. After transfer, the polyvinylidene difluoride membranes were probed using anti-RUNX1 (Cell Signaling Technology, Cat. #4334; RRID: AB_2184099), anti-HA antibody (Cell Signaling Technology, Cat. #26183; RRID: AB_10978021), and β-actin (Sigma-Aldrich, Cat. #A3854; RRID: AB_262011) and visualized using standard methods.

ASOs

ASOs were designed using 2′-O-methoxyethyl phosphorothioate chemistry to increase ASO stability and reduce off-target effects (IDT). For qPCR analysis, cells were collected 4 days after treatment with 500 nmol/L of control ASO or RUNX1C ASO by direct addition to the cell culture media. For annexin V analysis, cells were treated with ASOs 2 days before DMSO or cytarabine (500 nmol/L) treatment, treated for an additional 2 days, and then analyzed using flow cytometry.

p27K Quiescent Reporter

The p27K mutant from Oki and colleagues (59) was fused to mCherry-T2A-hygromycin, and EF1α promoter was synthesized as gene blocks by Twist Bioscience and cloned as a modular assembly using the Gibson Assembly into lentiviral backbone linearized by PmeI and BsrGI as previously described (71). Cells were selected using 200 μg/mL hygromycin.

Short-Read RNA-seq Preparation and Analysis

About 2×10^6 cDNA overexpressing RUNX1 isoforms in MOLM-13 cells was harvested 3 days after transduction and washed using 1× PBS. Total RNA was extracted using the RNeasy Plus Mini Kit (Qiagen, Cat. #74136) and QIAshredder (Qiagen, Cat. #79656) according to the manufacturer's protocol. We isolated poly(A) mRNA using the magnetic isolation method (New England Biolabs, Cat. #E7490S), using ~1 μg of total mRNA. To generate RNA-seq libraries, we used NEXTFLEX Rapid Directional (PerkinElmer) protocol and NEXTFLEX RNA-seq barcodes (PerkinElmer, Cat. #NOVA-5198-02), which were carried out according to the manufacturer's protocol. Library fragments were amplified with PCR, size-selected using AMPure XP Beads to select for fragments between 200 and 500 bps. RNA-seq barcoded libraries were then sequenced using NovaSeq X (150 paired end cycles).

RNA-seq reads were first mapped to the transcriptome annotations assembled as described above using RSEM v1.2.4 (72), modified to invoke Bowtie v1.0.0 (73) with the "-v 2" option. The remaining unaligned reads were then mapped to the genome hg38, and a database of possible splice junctions, consisting of all possible combinations of 5′ and 3′ ss, annotated for each gene using TopHat v2.0.8b (74). The resulting read alignments generated by TopHat were then merged with the output from the RSEM. The reads were filtered to ensure that splice junction–spanning reads had a minimum overhang of 6 nt. Additional information on sample barcodes can be found in Supplementary Table S5.

LR-seq Preparation and Poly(A) Tail Length Analysis

About 20×10^6 cells were collected and washed using 1× PBS. Total RNA was extracted using the RNeasy Plus Mini Kit (Qiagen, Cat. #74136) and QIAshredder (Qiagen, Cat. #79656) according to the manufacturer's protocol. Poly A-tailed RNA was enriched using the Dynabeads mRNA Purification Kit (Invitrogen, Cat # 61006). Libraries were prepared using the Direct RNA Sequencing Kit (Oxford Nanopore Technologies, SQK-RNA004), according to the manufacturer's recommendations. In brief, approximately 300 ng of poly(A) tailed RNA per sample was incubated with a reverse transcription (RT) adapter for 10 to 20 minutes at room temperature, followed by RT using SuperScript III Reverse Transcriptase (Thermo Fisher Scientific, Cat. #18080044) and Agencourt RNAClean XP Beads (Beckman Coulter). The eluted RT-RNA samples were then incubated with an RNA ligation adapter for 20 to 30 minutes at room temperature, followed by another RNAClean XP Bead cleanup. The completed libraries were quantified by fluorometry (Qubit, Thermo Fisher Scientific) and sequenced on RNA flow cells (FLO-PRO004RA) using a PromethION (Oxford Nanopore Technologies) for 72 hours. Live basecalling was performed during the experiment by using Guppy's high-accuracy basecalling model in MinKNOW. For direct RNA-seq data obtained from the nanopore platform, Dorado (Oxford Nanopore Technologies) was used to call the read sequences and estimate poly(A) tail length. Base-called reads with poly(A) tail length estimates were aligned against the human genome hg38 using Minimap2 (-ax splice -t 7 -B 3 -O 3,20 --junc-bed GENCODE v43 annotation) and then assigned to a unique gene using only the primary alignments by IsoQuant (--data_type nanopore --gene_quantification unique_only --splice_correction_strategy default_ont --no_secondary). Reads assigned to each gene were extracted to obtain the poly(A) tail length tags in R, and the Kolmogorov–Smirnov test was performed to detect the poly(A) tail length change between the control vector and BTG overexpression groups at the single gene level. The median poly(A) tail length was plotted at both the whole transcriptome and single gene levels to show the change between control and BTG overexpression samples.

CUT&RUN Preparation and Analysis

MOLM-13 cells were transduced with RUNX1 3×FLAG-tagged cDNA constructs linked to a GFP reporter, and 1 million cells per replicate were sorted to enrich for GFP-positive cells. CUT & RUN experiments were performed as described in the CUTANA CUT&RUN Kit (EpiCypher, Cat. #14-1048). Anti-FLAG M2 mAbs (Sigma-Aldrich, Cat. #F1804) were used in all experiments. Libraries were generated using the CUTANA CUT&RUN Library Prep Kit (EpiCypher, Cat. #14-1002) according to the manufacturer's protocol. Library quality was assessed using the High Sensitivity Bioanalyzer kit (Agilent), and libraries with different barcodes were pooled and sequenced on NovaSeq X. For CUT&RUN analysis, reads were aligned to the human genome hg38 using Bowtie 2 v2.4.5 (75), following the parameters as previously suggested (76): --very-sensitive-local --no-mixed --phred33 -I 10 -X 700 --no-discordant. Samtools v1.16.1 (77) was used to remove presumed PCR duplicates using the rmdup command, and BAM files containing uniquely mapped reads were created. The blacklist regions were obtained from the ENCODE blacklist and removed. Filtered BAM files were used for downstream analyses. Count per million–normalized bigWig files were created using the bamCoverage command with deepTools v3.5.4 and visualized on Integrative Genomics Viewer (v2.17.4). CUT&RUN signals were called on using MACS2 v2.2.7.1 (78) using the narrowPeak setting with a q value cutoff of 0.05. Genes proximal to the peaks were annotated against the hg38 genome using annotatePeaks.pl in HOMER v4.11 (79). RUNX1-binding motifs were identified using MEME-ChIP software. To compare differentially bound regions between WT and mutant RUNX1C, sorted BAM files and MACS2 peak calls for all biological replicates were analyzed using the DiffBind v3.12.0 package in R (v4.3.2). The two genotypes were compared using relative log expression (RLE) normalization with backgroundTRUE. Regions with an FDR <0.05 were considered significantly differentially bound, as determined using edgeR. Additional information on sample barcodes can be found in Supplementary Table S5.

Flow Cytometry

Cell-line suspensions were subjected to centrifugation at 400*g* for 5 minutes at 4°C, and the supernatant was discarded. Pellets were resuspended in 1 mL PBS with 2% FCS and filtered using a 70-μm nylon mesh (Thermo Fisher Scientific) with residual cell clumps discarded. After centrifuging at 400*g* and 4°C for 5 minutes, the supernatant was discarded, and the cell pellet was resuspended in PBS (Corning) with 2% FCS and placed on ice prior to staining for FACS. After antibody incubation, 0.1×10^6 cell suspensions were subjected to two wash cycles involving resuspension of cell pellets in 3 mL PBS with 2% FCS, followed by centrifuging at 400*g* at 4°C for 5 minutes, then supernatant removal. Finally, samples were resuspended in 300 μL of PBS with 2% FCS per 1×10^6 cells, supplemented with DAPI (0.5 μg/mL, MilliporeSigma, Cat. #D9542) for LIVE/DEAD staining. For the Ki-67 cell cycle assay, 1×10^6 cells were washed two times with PBS, the supernatant discarded, the cell pellets loosened by vortexing and resuspended in 3 mL cold 70% ethanol drop by drop to the cell pellet while vortexing, then incubated at −20°C for 1 hour. Subsequently, the cells were washed using Cell Staining Buffer and incubated with APC antihuman Ki-67 (BD Biosciences, Cat. #561277) in the ratio 1:100 at room temperature for 1 hour. Cells were washed two times with Cell Staining Buffer and incubated with 0.5 μg/mL DAPI for DNA content, followed by flow cytometry. For apoptosis assay, 0.1×10^6 cells were collected and washed two times with cold Annexin V Binding Buffer (BioLegend, Cat. #422201). They were resuspended in 100 μL Annexin V Binding Buffer. About 5 μL of APC Annexin V (BioLegend, Cat. #640941) and 0.5 μg/mL DAPI were added. The cells were gently vortexed and incubated for 15 minutes at room temperature in the dark. Then, 400 μL Annexin V Binding Buffer was added to each sample and analyzed by using flow cytometry. For OP-Puro incorporation assays, protein synthesis was measured using the Click-iT Plus OPP Alexa Fluor 647 Protein Synthesis Assay Kit (Thermo Fisher Scientific, Cat. #C10458), according to the manufacturer's protocol. Briefly, 0.1×10^6 AML cells transduced with BTG2 cDNA or control vector were incubated with or without 20 μmol/L Click-iT OPP (component A) for 30 minutes at 37°C and then fixed and permeabilized (BD Biosciences, Cat. #554714). Next, the Click-iT Plus OPP reaction cocktail was prepared according to the manufacturer's protocol; the permeabilization buffer was removed; and the cells were washed twice with PBS. The Click-iT Plus OPP reaction cocktail was added to the cells and incubated for 30 minutes at room temperature in the dark. The reaction cocktail was spun and removed, then washed once using reaction rinse buffer. The cells were resuspended in a cell-staining buffer containing DAPI. For flow cytometry analysis, samples were gated on the basis of the forward and side scatter, followed by exclusion of doublets, then gated on viable cells ($DAPI^{low}$). sgRNA, ectopic cDNA expression, or p27K-mCherry gating was based on fluorescence (GFP or mCherry) relative to non-transduced control cells. Appropriate unstained or single fluorophore controls were included to establish gates for each fluorochrome and ensure accurate discrimination of positive versus negative populations. All gating strategies were consistently applied across conditions, and nontargeting control sgRNAs or control vector served as internal controls to assess experimental variability and enable comparison between replicates. All the flow cytometry data analysis was performed using FACSDiva (BD Biosciences) and FlowJo (BD Biosciences) software.

Drug Treatment IC_{50} Measurements

Cell viability was determined using the CellTiter-Glo assay (Promega), according to the manufacturer's protocol. Briefly, 25,000 cells per well were plated in 96-well plates and exposed to the indicated compounds at various concentration ranges, with a minimum of three technical replicates per concentration per cell line. The plates were shaken for 15 minutes, and bioluminescence was determined using BioTek Synergy H1. The absolute viability values were converted to percentage viability and normalized to the DMSO control treatment. Normalized values were plotted using a nonlinear fit of log(inhibitor) versus response (four parameters) using GraphPad Prism v9.0 to obtain IC_{50} values.

qPCR Measurement of Gene Expression

RNA was extracted from the indicated cell lines and reverse transcribed into cDNA using the Verso cDNA Synthesis Kit (Thermo Fisher Scientific). Gene expression was measured using primers amplifying a coding sequence region and designed using Primer3 (https://bioinfo.ut.ee/primer3-0.4.0/), with *ACTB* as the housekeeping gene. Primers for the RUNX1 isoform were obtained from Challen and colleagues (15). Relative expression levels across cell lines were calculated using the ΔΔCt method as per standard procedures.

Targeted Amplicon Bisulfite Sequencing

MOLM-13 cells were collected, and DNA was extracted using the DNeasy Blood & Tissue Kit (Cat. #69504). About 2 μg of DNA was bisulfite treated using the EZ DNA Methylation-Gold Kit (Zymo Research, Cat. #D5005), according to the supplier's instructions. PCR was performed using KAPA HiFi HotStart ReadyMix (KAPA Biosystems, Cat. #KM2802), and the PCR products were cloned into the pCR4-TOPO TA vector according to the manufacturer's instructions (Thermo Fisher Scientific, Cat. #K4575J10). Subcloned colonies were sequenced using the M13 reverse primer (5′-CAGGAAACAGCTATGAC-3′).

RNA Stability

MOLM-13 cells were transduced with BTG2 overexpression or control vector and treated with 2.5 μg/mL actinomycin D (Sigma-Aldrich) 7 days after transduction. RNA was extracted at the indicated timepoints (0, 6, 8, and 10 hours) after transcription inhibition using the RNeasy Plus Mini Kit (Qiagen, Cat. #74316) according to the manufacturer's instructions and converted to cDNA using the High-Capacity RNA-to-cDNA Kit (Life Technologies, Cat. #4387406). RT-PCR was performed using Fast SYBR Green Plus Master Mix (Applied Biosystems). The target gene Ct values were normalized to 18S Ct values and used to calculate ΔCt. Relative mRNA abundance was calculated as the start of transcriptional inhibition [0-hour timepoint; $2 - (\Delta Ct - \Delta Ct^*)$] for each gene.

RNA Targeting of RUNX1C Isoform

RUNX1C-specific sgRNAs were designed using https://cas13design.nygenome.org/ and cloned into a pLenti sgRNA direct repeat vector (Addgene, plasmid number 138151). THP-1 or MOLM-13 RfxCas13d AML cell lines were transduced with sgRNAs and treated with 1 μg/mL doxycycline to activate RfxCas13d for 4 days, followed by qPCR analysis and CellTiter-Glo assays. For the RNAi experiments, shRNAs were designed using the Broad Institute GPP Web Portal, and sequences were cloned into a Tet-ON miR-E (miR-30 variant)–based vector (LT3GEPIR; Addgene, plasmid number 111177).

RNA-seq Read Mapping

RNA-seq reads were first mapped to the transcriptome annotations assembled as described above using RSEM v1.2.4 (72), modified to invoke Bowtie v1.0.0 (73) with the "-v 2" option. The remaining unaligned reads were then mapped to the genome and a database of possible splice junctions, consisting of all possible combinations of 5′ and 3′ ss annotated for each gene, using TopHat v2.0.8b (74). The resulting read alignments generated by TopHat were then merged with the output from the RSEM. The reads were filtered to ensure that splice junction–spanning reads had a minimum overhang of 6 nt.

Isoform and AS Analysis

Paired RNA-seq data of patients with AML were obtained from Li and colleagues (4) and downloaded from Database of Genotypes and Phenotypes (dbGaP) study phs001027. The only inclusion criterion applied was the use of bone marrow specimens, excluding peripheral blood samples, to ensure consistency and enrichment of leukemic blasts across patients. Annotations from the UCSC knownGene (80), Ensembl 71 (81), and MISO v2.0 (18) were combined to create a genome annotation for the human UCSC hg19 (GRCh37) assembly. All reads were mapped to the transcriptome using RSEM v1.2.4 (72) and the Bowtie alignment option "-v 2" (73). RSEM produces gene-level estimates of expression in units of transcripts per million. All gene expression estimates were normalized using the trimmed mean of M values method (82). Reads that failed to align were mapped to the genome using TopHat v2.0.8b (74), and an expanded annotation was created by computing all possible combinations of annotated 5′ and 3′ ss per gene. Salmon (17) v1.10.2 was used to map RNA-seq reads to a "gentrome" composed of GENCODE 43 cDNA sequences appended to GENCODE 43 genomic sequences. Salmon-generated transcripts-per-million expression matrices were used for comparing isoform expression levels between samples. We quantified splicing changes with MISO v2.0 (18) using combined RSEM and TopHat alignments as inputs. We used a two-sided t test to test for differential isoform expression between the sample groups. Differentially spliced events were defined as those with at least 20 isoform-identifying reads in each sample, a minimum absolute difference of 10% in isoform expression, and a P value < 0.05. All analyses were conducted within the R Programming environment using tools from Bioconductor (83). Visualizations were created using dplyr, ggplot2, and UpSetR (84) packages. Sashimi plots were generated using the Integrative Genomics Viewer of the Broad Institute.

DNA Methylation Analysis

Bisulfite sequencing data from the dbGaP study phs001027 (4) were downloaded and converted into FASTQ format using the SRA Toolkit (https://github.com/ncbi/sra-tools/wiki) v3.0.0. Examination of reports from FastQC (https://www.bioinformatics.babraham.ac.uk/projects/fastqc) v0.12.1 did not suggest contamination with sequencing adapters or other technical problems. Only paired bone marrow samples (diagnosis and relapse samples from the same patient) were analyzed. The only inclusion criterion applied was the use of bone marrow specimens, excluding peripheral blood samples, to ensure consistency and enrichment of leukemic blasts across patients. Sequences were mapped to the GRCh38.p13 (NCBI accession GCF_000001405.39) genomic assembly using Bismark (85) v0.24.1, calling Bowtie 2 (75) v2.5.0. Mapping data were imported into methylKit (86) v1.26.0, tabulating coverage for methylation positions aligned with at least three reads (with a Phred quality of at least 20 at the aligned position) from each of at least 10 samples. Only positions within the interval Chr21:34786301-36006167 were evaluated, corresponding to positions within 1,500 bases of the RUNX1 gene. Methylation differences between diagnosis and relapse at each of the resulting 809 tested positions were modeled using methylKit, including patient ID as a covariate. The effects of relapse on methylation were tested using χ^2 statistics, and FDRs were calculated using the Benjamini–Yekutieli procedure. An FDR cutoff of 0.05 was used to identify significance. The top 10 (sorted by q value) methylKit hits in the 3-kbp genomic interval chr21:34884999-34887999 were selected for analysis. At each of these 10 genomic positions, for each patient, we calculated the proportion 5-mc and the difference in 5-mc proportion between diagnosis and relapse. For each of the 10 genomic positions, a boxplot was made of the methylation differences between diagnosis and relapse.

Data Availability

RNA-seq reads for human AML samples (dbGaP study phs001027; ref. 4) were downloaded from the NCI Genomic Data Commons. RNA-seq for RUNX1 isoform expression was deposited in the Gene Expression Omnibus (GSE273034). CUT&RUN for RUNX1 isoforms was found in GSE273226. LR-seq data generated as part of this study were deposited in Gene Expression Omnibus (GSE273359). This article does not report original code. Any additional information required to reanalyze the data reported in this article is available from the lead contact upon request.

Authors' Disclosures

O. Abdel-Wahab reports grants and personal fees from Codify Therapeutics, AstraZeneca, and Minovia Therapeutics, other support from Envisagenics and Harmonic Discovery, and grants from Nurix Therapeutics outside the submitted work. R.K. Bradley reports grants, personal fees, and other support from Codify Therapeutics and other support from Synthesize Bio outside the submitted work. E. Wang reports other support from BlossomHill Therapeutics outside the submitted work. No disclosures were reported by the other authors.

Authors' Contributions

C. Han: Data curation, formal analysis, validation, investigation, visualization, methodology. **Z. Zhang:** Data curation, software, formal analysis, validation, investigation, visualization, methodology. **E.I. Crosse:** Software, formal analysis, validation, investigation, visualization. **S. Sajedi:** Data curation, software, formal analysis, validation, investigation, visualization, methodology. **B. Lu:** Formal analysis, investigation, visualization, methodology. **X. Wang:** Investigation, visualization, methodology. **S. Karma:** Validation, investigation, visualization, methodology. **M. Kostich:** Data curation, software, formal analysis, validation, investigation, visualization, methodology. **S.H. Rajendran:** Validation, investigation, visualization, methodology. **D.B. Udy:** Investigation. **S. Chen:** Investigation. **A. Arnuk:** Validation, investigation, visualization, methodology. **A.E. Lawal:** Validation, investigation, visualization. **K.R. Koenig:** Validation, investigation, visualization, methodology. **M. McKenna:** Validation, investigation, visualization, methodology. **P.K. Reville:** Validation, investigation, visualization, methodology. **H.A. Abbas:** Data curation, software, validation, investigation, visualization, methodology. **O. Abdel-Wahab:** Conceptualization, supervision, validation, investigation, visualization, methodology. **P. Miura:** Data curation, software, formal analysis, validation, investigation, visualization, methodology. **R.K. Bradley:** Conceptualization, data curation, software, formal analysis, supervision, validation, investigation, visualization, methodology. **E. Wang:** Conceptualization, resources, data curation, software, formal analysis, supervision, funding acquisition, validation, investigation, visualization, methodology, writing–original draft, project administration, writing–review and editing.

Acknowledgments

We thank all the members of the Wang Laboratory for their discussions throughout this project. We acknowledge the assistance from Genome Technologies Sequencing, Computational Sciences, and Flow Cytometry Services at The Jackson Laboratory (JAX). We also thank Dr. Bo Reese and the UConn Center for Genome Innovation for their assistance with the sequencing. E. Wang was supported by JAX Cancer Center New Investigator Award (P30CA034196), JAX start-up funds, JAX Cancer Center Fast Forward Award, the Leukemia Research Foundation, and the Butler Family Foundation. E.I. Crosse is a Damon Runyon Cancer Research Foundation Fellow. This work was supported by National Institute of General Medical

Sciences grant R35GM138319 awarded to P. Miura. H.A. Abbas is supported by the Physician Scientist Award from the MD Anderson Cancer Center and the Cancer Prevention and Research Institute of Texas Individual Investigator Award. P.K. Reville was supported by a postdoctoral fellowship from the Lymphoma Research Foundation. O. Abdel-Wahab was supported by the NIH/NCI (R01 CA242020 and P50 CA254838-01) and Leukemia and Lymphoma Society. O. Abdel-Wahab and R.K. Bradley were supported by the Edward P. Evans Foundation, NCI (R01 CA251138 and R01 CA283364), and National Heart Lung and Blood Institute (R01 HL128239).

Note

Supplementary data for this article are available at Blood Cancer Discovery Online (https://bloodcancerdiscov.aacrjournals.org/).

Received November 20, 2024; revised February 20, 2025; accepted July 8, 2025; posted first July 9, 2025.

REFERENCES

1. Short NJ, Rytting ME, Cortes JE. Acute myeloid leukaemia. Lancet 2018;392:593–606.
2. Ebinger S, Özdemir EZ, Ziegenhain C, Tiedt S, Castro Alves C, Grunert M, et al. Characterization of rare, dormant, and therapy-resistant cells in acute lymphoblastic leukemia. Cancer Cell 2016;30:849–62.
3. Lawrence MS, Stojanov P, Mermel CH, Robinson JT, Garraway LA, Golub TR, et al. Discovery and saturation analysis of cancer genes across 21 tumour types. Nature 2014;505:495–501.
4. Li S, Garrett-Bakelman FE, Chung SS, Sanders MA, Hricik T, Rapaport F, et al. Distinct evolution and dynamics of epigenetic and genetic heterogeneity in acute myeloid leukemia. Nat Med 2016;22:792–9.
5. Calderon A, Han C, Karma S, Wang E. Non-genetic mechanisms of drug resistance in acute leukemias. Trends Cancer 2024;10:38–51.
6. Zeng AGX, Bansal S, Jin L, Mitchell A, Chen WC, Abbas HA, et al. A cellular hierarchy framework for understanding heterogeneity and predicting drug response in acute myeloid leukemia. Nat Med 2022;28:1212–23.
7. Wang E, Pineda JMB, Kim WJ, Chen S, Bourcier J, Stahl M, et al. Modulation of RNA splicing enhances response to BCL2 inhibition in leukemia. Cancer Cell 2023;41:164–80.e8.
8. Morales ML, García-Vicente R, Rodríguez-García A, Reyes-Palomares A, Vincelle-Nieto Á, Álvarez N, et al. Posttranslational splicing modifications as a key mechanism in cytarabine resistance in acute myeloid leukemia. Leukemia 2023;37:1649–59.
9. Kim J-H, Baddoo MC, Park EY, Stone JK, Park H, Butler TW, et al. SON and its alternatively spliced isoforms control MLL complex-mediated H3K4me3 and transcription of leukemia-associated genes. Mol Cell 2016;61:859–73.
10. Wang E, Lu SX, Pastore A, Chen X, Imig J, Chun-Wei Lee S, et al. Targeting an RNA-binding protein network in acute myeloid leukemia. Cancer Cell 2019;35:369–84.e7.
11. Scarpato M, Federico A, Ciccodicola A, Costa V. Novel transcription factor variants through RNA-sequencing: the importance of being "alternative". Int J Mol Sci 2015;16:1755–71.
12. Okuda T, van Deursen J, Hiebert SW, Grosveld G, Downing JR. AML1, the target of multiple chromosomal translocations in human leukemia, is essential for normal fetal liver hematopoiesis. Cell 1996;84:321–30.
13. Ichikawa M, Asai T, Saito T, Seo S, Yamazaki I, Yamagata T, et al. AML-1 is required for megakaryocytic maturation and lymphocytic differentiation, but not for maintenance of hematopoietic stem cells in adult hematopoiesis. Nat Med 2004;10:299–304.
14. Sood R, Kamikubo Y, Liu P. Role of RUNX1 in hematological malignancies. Blood 2017;129:2070–82.
15. Challen GA, Goodell MA. Runx1 isoforms show differential expression patterns during hematopoietic development but have similar functional effects in adult hematopoietic stem cells. Exp Hematol 2010;38:403–16.
16. Gialesaki S, Bräuer-Hartmann D, Issa H, Bhayadia R, Alejo-Valle O, Verboon L, et al. RUNX1 isoform disequilibrium promotes the development of trisomy 21-associated myeloid leukemia. Blood 2023;141:1105–18.
17. Patro R, Duggal G, Love MI, Irizarry RA, Kingsford C. Salmon provides fast and bias-aware quantification of transcript expression. Nat Methods 2017;14:417–9.
18. Katz Y, Wang ET, Airoldi EM, Burge CB. Analysis and design of RNA sequencing experiments for identifying isoform regulation. Nat Methods 2010;7:1009–15.
19. Demircioğlu D, Cukuroglu E, Kindermans M, Nandi T, Calabrese C, Fonseca NA, et al. A pan-cancer transcriptome analysis reveals pervasive regulation through alternative promoters. Cell 2019;178:1465–77.e17.
20. Ghozi MC, Bernstein Y, Negreanu V, Levanon D, Groner Y. Expression of the human acute myeloid leukemia gene AML1 is regulated by two promoter regions. Proc Natl Acad Sci U S A 1996;93:1935–40.
21. Owens DDG, Anselmi G, Oudelaar AM, Downes DJ, Cavallo A, Harman JR, et al. Dynamic Runx1 chromatin boundaries affect gene expression in hematopoietic development. Nat Commun 2022;13:773.
22. Webber BR, Iacovino M, Choi SH, Tolar J, Kyba M, Blazar BR. DNA methylation of Runx1 regulatory regions correlates with transition from primitive to definitive hematopoietic potential in vitro and in vivo. Blood 2013;122:2978–86.
23. Sroczynska P, Lancrin C, Kouskoff V, Lacaud G. The differential activities of Runx1 promoters define milestones during embryonic hematopoiesis. Blood 2009;114:5279–89.
24. Levanon D, Glusman G, Bangsow T, Ben-Asher E, Male DA, Avidan N, et al. Architecture and anatomy of the genomic locus encoding the human leukemia-associated transcription factor RUNX1/AML1. Gene 2001;262:23–33.
25. Miyoshi H, Ohira M, Shimizu K, Mitani K, Hirai H, Imai T, et al. Alternative splicing and genomic structure of the AML1 gene involved in acute myeloid leukemia. Nucleic Acids Res 1995;23:2762–9.
26. Duy C, Li M, Teater M, Meydan C, Garrett-Bakelman FE, Lee TC, et al. Chemotherapy induces senescence-like resilient cells capable of initiating AML recurrence. Cancer Discov 2021;11:1542–61.
27. Saito Y, Kitamura H, Hijikata A, Tomizawa-Murasawa M, Tanaka S, Takagi S, et al. Identification of therapeutic targets for quiescent, chemotherapy-resistant human leukemia stem cells. Sci Transl Med 2010;2:17ra9.
28. Lee SE, Sada A, Zhang M, McDermitt DJ, Lu SY, Kemphues KJ, et al. High Runx1 levels promote a reversible, more-differentiated cell state in hair-follicle stem cells during quiescence. Cell Rep 2014;6:499–513.
29. Marion W, Koppe T, Chen C-C, Wang D, Frenis K, Fierstein S, et al. RUNX1 mutations mitigate quiescence to promote transformation of hematopoietic progenitors in Fanconi anemia. Leukemia 2023;37:1698–708.
30. Hwang SS, Lim J, Yu Z, Kong P, Sefik E, Xu H, et al. mRNA destabilization by BTG1 and BTG2 maintains T cell quiescence. Science 2020;367:1255–60.
31. Jia W, Kong L, Kidoya H, Naito H, Muramatsu F, Hayashi Y, et al. Indispensable role of Galectin-3 in promoting quiescence of hematopoietic stem cells. Nat Commun 2021;12:2118.
32. Gurumurthy S, Xie SZ, Alagesan B, Kim J, Yusuf RZ, Saez B, et al. The Lkb1 metabolic sensor maintains haematopoietic stem cell survival. Nature 2010;468:659–63.
33. Brady G, Elgueta Karstegl C, Farrell PJ. Novel function of the unique N-terminal region of RUNX1c in B cell growth regulation. Nucleic Acids Res 2013;41:1555–68.
34. Papaemmanuil E, Gerstung M, Bullinger L, Gaidzik VI, Paschka P, Roberts ND, et al. Genomic classification and prognosis in acute myeloid leukemia. N Engl J Med 2016;374:2209–21.
35. Zuber J, Radtke I, Pardee TS, Zhao Z, Rappaport AR, Luo W, et al. Mouse models of human AML accurately predict chemotherapy response. Genes Dev 2009;23:877–89.
36. Lasry A, Nadorp B, Fornerod M, Nicolet D, Wu H, Walker CJ, et al. An inflammatory state remodels the immune microenvironment and improves risk stratification in acute myeloid leukemia. Nat Cancer 2023;4:27–42.

37. Yeaton A, Cayanan G, Loghavi S, Dolgalev I, Leddin EM, Loo CE, et al. The impact of inflammation-induced tumor plasticity during myeloid transformation. Cancer Discov 2022;12:2392–413.
38. Li Q, Lai Q, He C, Zhang H, Pan X, Li H, et al. RUNX1 regulates the proliferation and chemoresistance of colorectal cancer through the Hedgehog signaling pathway. J Cancer 2021;12:6363–71.
39. Ebner J, Schmoellerl J, Piontek M, Manhart G, Troester S, Carter BZ, et al. ABCC1 and glutathione metabolism limit the efficacy of BCL-2 inhibitors in acute myeloid leukemia. Nat Commun 2023; 14:5709.
40. Skene PJ, Henikoff S. An efficient targeted nuclease strategy for high-resolution mapping of DNA binding sites. Elife 2017;6: e21856.
41. Simeoni F, Romero-Camarero I, Camera F, Amaral FMR, Sinclair OJ, Papachristou EK, et al. Enhancer recruitment of transcription repressors RUNX1 and TLE3 by mis-expressed FOXC1 blocks differentiation in acute myeloid leukemia. Cell Rep 2021;36: 109725.
42. Huang G, Zhang P, Hirai H, Elf S, Yan X, Chen Z, et al. PU.1 is a major downstream target of AML1 (RUNX1) in adult mouse hematopoiesis. Nat Genet 2008;40:51–60.
43. Ma W, Noble WS, Bailey TL. Motif-based analysis of large nucleotide data sets using MEME-ChIP. Nat Protoc 2014;9:1428–50.
44. Liu H, Carlsson L, Grundström T. Identification of an N-terminal transactivation domain of Runx1 that separates molecular function from global differentiation function. J Biol Chem 2006;281: 25659–69.
45. Tyner JW, Tognon CE, Bottomly D, Wilmot B, Kurtz SE, Savage SL, et al. Functional genomic landscape of acute myeloid leukaemia. Nature 2018;562:526–31.
46. Ishikawa F, Yoshida S, Saito Y, Hijikata A, Kitamura H, Tanaka S, et al. Chemotherapy-resistant human AML stem cells home to and engraft within the bone-marrow endosteal region. Nat Biotechnol 2007;25:1315–21.
47. Boyd AL, Aslostovar L, Reid J, Ye W, Tanasijevic B, Porras DP, et al. Identification of chemotherapy-induced leukemic-regenerating cells reveals a transient vulnerability of human AML recurrence. Cancer Cell 2018;34:483–98.e5.
48. Kim SH, Jung IR, Hwang SS. Emerging role of anti-proliferative protein BTG1 and BTG2. BMB Rep 2022;55:380–8.
49. Passeri D, Marcucci A, Rizzo G, Billi M, Panigada M, Leonardi L, et al. Btg2 enhances retinoic acid-induced differentiation by modulating histone H4 methylation and acetylation. Mol Cell Biol 2006;26: 5023–32.
50. Stupfler B, Birck C, Séraphin B, Mauxion F. BTG2 bridges PABPC1 RNA-binding domains and CAF1 deadenylase to control cell proliferation. Nat Commun 2016;7:10811.
51. Ameerul A, Almasmoum H, Pavanello L, Dominguez C, Winkler GS. Structural model of the human BTG2-PABPC1 complex by combining mutagenesis, NMR chemical shift perturbation data and molecular docking. J Mol Biol 2022;434:167662.
52. Wang Y, Zhao Y, Bollas A, Wang Y, Au KF. Nanopore sequencing technology, bioinformatics and applications. Nat Biotechnol 2021; 39:1348–65.
53. Mauxion F, Faux C, Séraphin B. The BTG2 protein is a general activator of mRNA deadenylation. EMBO J 2008;27:1039–48.
54. Subtelny AO, Eichhorn SW, Chen GR, Sive H, Bartel DP. Poly(A)-tail profiling reveals an embryonic switch in translational control. Nature 2014;508:66–71.
55. Lima SA, Chipman LB, Nicholson AL, Chen Y-H, Yee BA, Yeo GW, et al. Short poly(A) tails are a conserved feature of highly expressed genes. Nat Struct Mol Biol 2017;24:1057–63.
56. Signer RAJ, Magee JA, Salic A, Morrison SJ. Haematopoietic stem cells require a highly regulated protein synthesis rate. Nature 2014;509: 49–54.
57. Webster MW, Chen Y-H, Stowell JAW, Alhusaini N, Sweet T, Graveley BR, et al. mRNA deadenylation is coupled to translation rates by the differential activities of Ccr4-not nucleases. Mol Cell 2018;70: 1089–100.e8.
58. Chavez JS, Rabe JL, Loeffler D, Higa KC, Hernandez G, Mills TS, et al. PU.1 enforces quiescence and limits hematopoietic stem cell expansion during inflammatory stress. J Exp Med 2021;218:e20201169.
59. Oki T, Nishimura K, Kitaura J, Togami K, Maehara A, Izawa K, et al. A novel cell-cycle-indicator, mVenus-p27K-identifies quiescent cells and visualizes G0-G1 transition. Sci Rep 2014;4:4012.
60. Growney JD, Shigematsu H, Li Z, Lee BH, Adelsperger J, Rowan R, et al. Loss of Runx1 perturbs adult hematopoiesis and is associated with a myeloproliferative phenotype. Blood 2005;106:494–504.
61. Wessels H-H, Méndez-Mancilla A, Guo X, Legut M, Daniloski Z, Sanjana NE. Massively parallel Cas13 screens reveal principles for guide RNA design. Nat Biotechnol 2020;38:722–7.
62. Shi P, Murphy MR, Aparicio AO, Kesner JS, Fang Z, Chen Z, et al. Collateral activity of the CRISPR/RfxCas13d system in human cells. Commun Biol 2023;6:334.
63. Wesely J, Kotini AG, Izzo F, Luo H, Yuan H, Sun J, et al. Acute myeloid leukemia iPSCs reveal a role for RUNX1 in the maintenance of human leukemia stem cells. Cell Rep 2020;31:107688.
64. Sharma A, Mistriel-Zerbib S, Najar RA, Engal E, Bentata M, Taqatqa N, et al. Isoforms of the TAL1 transcription factor have different roles in hematopoiesis and cell growth. PLoS Biol 2023;21:e3002175.
65. Bourdon J-C, Fernandes K, Murray-Zmijewski F, Liu G, Diot A, Xirodimas DP, et al. p53 isoforms can regulate p53 transcriptional activity. Genes Dev 2005;19:2122–37.
66. Vadakekolathu J, Minden MD, Hood T, Church SE, Reeder S, Altmann H, et al. Immune landscapes predict chemotherapy resistance and immunotherapy response in acute myeloid leukemia. Sci Transl Med 2020;12:eaaz0463.
67. Wang B, Reville PK, Yassouf MY, Jelloul FZ, Ly C, Desai PN, et al. Comprehensive characterization of IFNγ signaling in acute myeloid leukemia reveals prognostic and therapeutic strategies. Nat Commun 2024;15:1821.
68. Kortylewski M, Swiderski P, Herrmann A, Wang L, Kowolik C, Kujawski M, et al. In vivo delivery of siRNA to immune cells by conjugation to a TLR9 agonist enhances antitumor immune responses. Nat Biotechnol 2009;27:925–32.
69. Tsui K-H, Chiang K-C, Lin Y-H, Chang K-S, Feng T-H, Juang H-H. BTG2 is a tumor suppressor gene upregulated by p53 and PTEN in human bladder carcinoma cells. Cancer Med 2018;7:184–95.
70. Townsend EC, Murakami MA, Christodoulou A, Christie AL, Köster J, DeSouza TA, et al. The public repository of xenografts enables discovery and randomized phase II-like trials in mice. Cancer Cell 2016;29:574–86.
71. Akama-Garren EH, Joshi NS, Tammela T, Chang GP, Wagner BL, Lee DY, et al. A modular assembly platform for rapid generation of DNA constructs. Sci Rep 2016;6:16836.
72. Li B, Dewey CN. RSEM: accurate transcript quantification from RNA-Seq data with or without a reference genome. BMC bioinformatics 2011;12:323.
73. Langmead B, Trapnell C, Pop M, Salzberg SL. Ultrafast and memory-efficient alignment of short DNA sequences to the human genome. Genome Biol 2009;10:R25.
74. Trapnell C, Pachter L, Salzberg SL. TopHat: discovering splice junctions with RNA-Seq. Bioinformatics 2009;25:1105–11.
75. Langmead B, Salzberg SL. Fast gapped-read alignment with Bowtie 2. Nat Methods 2012;9:357–9.
76. Skene PJ, Henikoff JG, Henikoff S. Targeted in situ genome-wide profiling with high efficiency for low cell numbers. Nat Protoc 2018; 13:1006–19.
77. Li H, Handsaker B, Wysoker A, Fennell T, Ruan J, Homer N, et al. The Sequence Alignment/Map format and SAMtools. Bioinformatics 2009;25:2078–9.
78. Zhang Y, Liu T, Meyer CA, Eeckhoute J, Johnson DS, Bernstein BE, et al. Model-based analysis of ChIP-seq (MACS). Genome Biol 2008;9:R137.
79. Heinz S, Benner C, Spann N, Bertolino E, Lin YC, Laslo P, et al. Simple combinations of lineage-determining transcription factors prime cis-regulatory elements required for macrophage and B cell identities. Mol Cell 2010;38:576–89.

80. Meyer LR, Zweig AS, Hinrichs AS, Karolchik D, Kuhn RM, Wong M, et al. The UCSC Genome Browser database: extensions and updates 2013. Nucleic Acids Res 2013;41:D64–9.
81. Flicek P, Ahmed I, Amode MR, Barrell D, Beal K, Brent S, et al. Ensembl 2013. Nucleic Acids Res 2013;41:D48–55.
82. Robinson MD, Oshlack A. A scaling normalization method for differential expression analysis of RNA-seq data. Genome Biol 2010;11:R25.
83. Huber W, Carey VJ, Gentleman R, Anders S, Carlson M, Carvalho BS, et al. Orchestrating high-throughput genomic analysis with Bioconductor. Nat Methods 2015;12:115–21.
84. Conway JR, Lex A, Gehlenborg N. UpSetR: an R package for the visualization of intersecting sets and their properties. Bioinformatics 2017;33:2938–40.
85. Krueger F, Andrews SR. Bismark: a flexible aligner and methylation caller for Bisulfite-Seq applications. Bioinformatics 2011;27:1571–2.
86. Akalin A, Kormaksson M, Li S, Garrett-Bakelman FE, Figueroa ME, Melnick A, et al. methylKit: a comprehensive R package for the analysis of genome-wide DNA methylation profiles. Genome Biol 2012;13:R87.